IEEE Access
Multidisciplinary ⋮ Rapid Review ⋮ Open Access Journal

Received March 6, 2022, accepted March 12, 2022, date of publication March 16, 2022, date of current version April 1, 2022.

Digital Object Identifier 10.1109/ACCESS.2022.3159973

A Quantitative Study of Non-Linear Convective Heat Transfer Model by Novel Hybrid Heuristic Driven Neural Soft Computing

MUHAMMAD FAWAD KHAN[1], MUHAMMAD SULAIMAN[1], CARLOS ANDRÉS TAVERA ROMERO[2], AND FAHAD SAMEER ALSHAMMARI[3]

[1]Department of Mathematics, Abdul Wali Khan University Mardan, Mardan, Khyber Pakhtunkhwa 23200, Pakistan
[2]COMBA Research and Development Laboratory, Faculty of Engineering, Universidad Santiago de Cali, Cali 76001, Colombia
[3]Department of Mathematics, College of Science and Humanities in Alkharj, Prince Sattam Bin Abdulaziz University, Al-Kharj 11942, Saudi Arabia

Corresponding author: Muhammad Sulaiman (msulaiman@awkum.edu.pk)

This work was supported by the Dirección General de Investigaciones of Universidad Santiago de Cali under Call 01-2021.

ABSTRACT Heat transfer has a vital role in material selection, machinery efficacy, and energy consumption. The notion of heat transfer is essential in understanding many phenomena related to several engineering fields. Particularly, Mechanical, civil and chemical engineering. The presentation of the heat transfer model in this manuscript is a dedication to the heat transfer characteristics such as conduction, convection, and radiation. The heat energy consumption mainly depends on these characteristics. A better conductive and convective paradigm is required for miniaturization of heat loss or transfer. The phenomenon is mathematically assumed with the required parameters. A new mathematical strategy is also designed and implemented in the manuscript to evaluate the dynamics of heat transfer model. The mathematical approach is the hybrid structure of the Sine-Cosine algorithm and Interior point algorithm. The validation of new technique is evaluated by mean absolute deviation, root mean square errors, and error in Nash–Sutcliffe efficiency. For better illustration, an extensive data set executed by the proposed mathematical strategy is also drawn graphically with convergence plots.

INDEX TERMS Interior point technique, machine learning, heat transfer, differential equation, quantitative analysis, neural network, mathematical model, hybridization.

I. INTRODUCTION

With the increase in energy consumption, the miniaturization of heat loss and heat transfer on surfaces and in devices surge the interest of researchers. To improve thermal performance, the researchers work in many engineering applications like thermal energy storage, heat transfer exchangers, Solar collectors, thermal control in electronic devices, etc. These researches contribute to minimizing the consumption of heat energy. In this regard, many best insulators are developed to lower energy consumption, which is considered a better strategy to minimize energy consumption. Various types of insulators are reported by [1]. For heat transfer applications, the understanding of its characteristics and determination of thermal properties in different shaped materials. That's why researchers explore heat transfer by convection, conduction, and radiations. Natural convection, radiation, and conduction are associated with diverse engineering applications [2]. Many researches studied natural convection mechanism in different thermal materials based on various conditions such as under the influence of magnetic field convection is studied by [3], [4], porous media saturatedi fluids studied and reported in [5]. Qi et al reported a study on the cooling process of high heat loss in electronic devices, such as CPUs. In this work, they said that magnetic field intensity could improve the heat exchanger efficiency [6], Nonlinear radiation and cross-diffusion effects on the micropolar nanoliquid flow past a stretching sheet with an exponential heat source [7], nonlinear Boussinesq approximation and non-uniform heat source/sink on nanoliquid flow with convective heat condition:sensitivity analysis [8]. In this article heat transfer is studied in $Ti_2 - EG$ with passive and active controlling of nano-particles [9] while the significance of inclination of magnetic field with nonlinear thermal radiation and

The associate editor coordinating the review of this manuscript and approving it for publication was Inês Domingues.

exponential space based heat source is reported in [8]. In [10] Nazeer *et al.* report the impact of on velocity and heat profiles. The numerical results in this study reveal that the velocity profile vanished by non-Newtonian terms and other parameters like magnetic field, viscosity and electro-kinetic while the behavior of velocity versus pressure gradient is opposite. Additionally, the temperature profile increases against the Brinkman number, pressure gradient, Joule heating, wall's temperature, viscosity while reverse behavior is observed via electro-kinetic and magnetic field parameters, heat transportation generation/absorption and radiative heat flux in homogeneous–heterogeneous catalytic reactions of non-Newtonian fluid is studied by [11], radiative flow by convective cylinder is studied in [12], comparative study of nano-particles in viscous fluid flow is reported in [13] and Ijaz Khan *et al.* reported study of reactive aspect in flow of tangent hyperbolic material [14]. For conduction phenomena, in [15] Unger *et al.* introduce a novel fin tube exchanger for the improvement of conductive heat transfer in the tube fins. At the same time, convection occurs along its surface. Rathod and Modi present numerical phenomena for the evaluation of thermo-fluid mechanism in a fin heat exchanger consisting of sinusoidal and elliptic winglets [16]. For heat conduction, employment of Eulerian-Lagrangian scheme for hydraulic characteristics of hybrid nanofluid flow inside the micro-pin-fins heat sink is discus by Ambreen *et al.* in [17]. As conduction and convection, radiation also has a contribution to heat transfer. Inquiring fin parameters and natural convection also deal with heat transfer with radiations. Heat transfer has many application such as PCM pipe bank thermal storage for space heating [18], Thermal performance of self-rewetting gold nanofluids [19], heat pipe cooled device with thermo-electric generator for nuclear power application [20], etc.

For such problems researcher introduce many numerical techniques or solved by existent techniques like Entropy generation and heat transfer analysis by Finite difference method [21]. Numerical and experimental analysis of resin-flow, heat-transfer [22], Computational modeling and analysis on rotating stretched disk flow with heat transfer [23]. Classical techniques need many information like initial point, gradient, feasible range, etc. But the global search techniques need a little information about the problem; such characteristics grab the researcher's interest. Many research introduces the implementation of meta-heuristics. These meta-heuristics are applicable to heat transfer problems and can be applied to solve a wide range of other engineering problems. A few of them are, supervised learning method for reconstruction in heat transfer problem [24], A physics-informed machine learning approach for solving heat transfer equation [25], heat transfer in a grooved pipe model by Stochastic Algorithms [26] with this the many hybridizations of unsupervised and supervised techniques are also reported in the literature. Analysis of temperature profiles in longitudinal fin is presented in [27], heat and entropy generation in flow of non-Newtonian fluid is analysed by Artificial neural networking (ANN) in [28], temperature distribution in convective straight fins [29], Multi order Fractional Differential Equations [30], Restoring Moment and Damping Effects Using Neuro-evolutionary Technique [31], non-linear MHD Jeffery–Hamel blood flow model, Optimal power flow solution in power systems [32], [33], Falkner–Skan flow problem is solved by SCA-SQP in [34], unipolar pump flow is evaluated by ANN-SCA-SQP by [35]. In a similar context of heat transfer, this work discusses the conductive, convective, and radiative heat transfer model in a fin. The work discusses different scenarios of conductive, convective, and radiative heat transfer combinations. The presented work is given as:

- The mathematical model of conductive, convective, and radiative heat transfer is presented.
- For the solution of the presented mathematical model Artificial Neural Network (ANN) is utilized with the hybridization paradigm of Sine-Cosine Algorithm(SCA) with Interior-point algorithm(IPA) abbreviated as ANN–SCA-IPA.
- The Dynamics of the model are evaluated by the variation of coefficient conductive, radiative and convective in the heat transfer model (HTM).
- The HTM is transformed into an optimization problem with a fitness function that uses the least square errors phenomena.
- Additionally, the ANN–SCA–IPA paradigm is evaluated by various statistical operators.

The structure of rest of paper is followed by section II which present formulation of HTM, section III present construction and discuses the ANN base HTM, section IV discusses the designing of fitness function, section V consist of hybridization paradigm, section VI define and explain performance operators, section VII discuss empirical results of HTM, section VIII consist of discussion on performance of ANN–SCA–IPA algorithm and section IX conclude the work.

II. FORMULATION OF NONLINEAR HEAT TRANSFER MODEL

Consider a fin having length b with cross section area A and thermal dependent conductivity as shown in Figure 1. It is considered that fin is relatively long as compare to A and is made up of isotropic solid material. On the surface heat is transfers through convection and radiation while at the bottom uniform temperature is considered while the tip of fin has negligible heat transfer. The transfer of heat on the surface of fins satisfies Stefan-Boltzmann's law. The thermal conductivity $k(T)$ in the fin is depend on the temperature which is defined as [36]

$$k = k_a \left[1 + \beta \left(T - T_a\right)\right], \tag{1}$$

where T_a denotes ambient temperature, inner temperature of fin is represented by T, temperature variation is denoted by β. Whenever $(T = T_a)$ the equation (1) reduced to $k = k_a$ which denotes thermal conductivity. The heat transfer model is analyzing the convective, conductive and radiative heat transfer mechanism in a longitudinal fin and perimeter P.

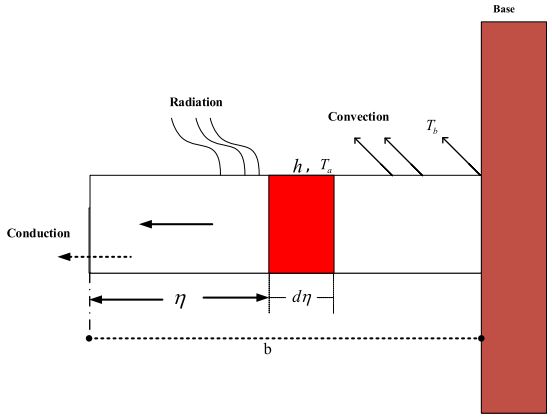

FIGURE 1. Physical structure of heat transfer model.

The efficient sink temperature for radiative heat transfer is T_s and fin's base temperature is T_b. The convection heat transfer coefficient h and the surface emissivity coefficient E_g are assumed to be constants, whereas the conduction coefficient k varies. As the fin is longitudinal, that's why it satisfy one dimensional heat transfer equation and boundary conditions are as follows: [37]–[39]:

$$\frac{\mathrm{d}}{\mathrm{d}\eta}\left(k\frac{\mathrm{d}T}{\mathrm{d}\eta}\right)-\frac{hp}{A}(T-T_a)-\frac{E_g\sigma}{A}\left(T^4-T_s^4\right)=0 \tag{2}$$

$$\frac{\mathrm{d}T}{\mathrm{d}\eta}=0 \text{ at } \eta=0, \text{ and } T=T_b \text{ at } \eta=b. \tag{3}$$

To make the equation dimensionless following new parameters are defined as

$$\begin{aligned}\theta&=\frac{T}{T_b},\quad \theta_a=\frac{T_a}{T_b},\quad \theta_s=\frac{T_s}{T_b}\\ \eta&=\frac{\eta}{b},\quad \nu^2=\frac{hpb^2}{k_aA},\quad \varepsilon_1=\beta T_b,\\ \varepsilon_2&=\frac{E_g\sigma T_b^3pb^3}{k_aA},\end{aligned} \tag{4}$$

here, ε_1 is heat conduction, ε_2 is heat radiation and ν is heat convection. By putting equation (1) into equation (2) and if $\theta_a=\theta_s=0$, then:

$$\frac{\mathrm{d}}{\mathrm{d}\eta}\left[(1+\epsilon_1\theta)\frac{\mathrm{d}\theta}{\mathrm{d}\eta}\right]-\nu^2\theta-\epsilon_2\theta^4=0 \tag{5}$$

$$\frac{\mathrm{d}\theta}{\mathrm{d}\eta}=0 \text{ at } \eta=0 \text{ and } \theta=1 \text{ at } \eta=1 \tag{6}$$

III. ARTIFICIAL NEURAL NETWORK BASED STRUCTURE OF THE HEAT TRANSFER MODEL

This section discusses the mathematical strategy for the approximation of heat transfer. The procedure is approximated by feed-forward neural network in terms of activation function log-sigmoid given in below equation:

$$\phi(x)=\frac{1}{1+e^{-x}}, \tag{7}$$

The feed-forward is simple and unidirectional network. It's computationally sound and simple to utilize. Additionally, The approximated trail solution $\hat{\theta}(\eta)$ and its derivatives first, second, third, and n^{th} order $\hat{\theta}'(\eta)$, $\hat{\theta}''(\eta)$, $\hat{\theta}'''(\eta)$ and $\hat{\theta}^n(\eta)$, respectively, for heat transfer procedure in equation (5) are presented in equation (8)

$$\begin{aligned}\hat{\theta}(\eta)&=\sum_{i=1}^{k}a_i\phi(w_i(\eta)+\zeta_i),\\ \hat{\theta}'(\eta)&=\sum_{i=1}^{k}a_i\phi'(w_i(\eta)+\zeta_i),\\ \hat{\theta}''(\eta)&=\sum_{i=1}^{k}a_i\phi''(w_i(\eta)+\zeta_i)\\ &\vdots\\ \hat{\theta}^n(\eta)&=\sum_{i=1}^{k}a_i\phi^n(w_i(\eta)+\zeta_i),\end{aligned} \tag{8}$$

in the model (8), number of neurons are denoted by k which must be multiple of three because the set $\mathbf{W}=[\mathbf{a},\quad \mathbf{w},\quad \zeta]$ consist of three components of neurons $\mathbf{a},\quad \mathbf{w},\quad \zeta$. Where $\mathbf{a}=[a_1,a_2,\ldots,a_k]$, $\mathbf{w}=[w_1,w_2,\ldots,w_k]$ and $\zeta=[\zeta_1,\zeta_2,\ldots,\zeta_k]$.

As heat transfer equation (5) is second order ordinary differential equation (ODE), so the putting equations (9)-(11) in equation (5)

$$\hat{\theta}(\eta)=\sum_{i=1}^{k}a_i\left(\frac{1}{1+e^{-(w_i\eta+b_i)}}\right), \tag{9}$$

$$\hat{\theta}'(\eta)=\sum_{i=1}^{k}a_iw_i\left(\frac{e^{-(w_i\eta+b_i)}}{(1+e^{-(w_i\eta+b_i)})^2}\right), \tag{10}$$

$$\hat{\theta}''=\sum_{i=1}^{k}a_iw_i^2\left(\frac{2e^{-2(w_i\eta+b_i)}}{\left(1+e^{-(w_i\eta+b_i)}\right)^3}-\frac{e^{-(w_i\eta+b_i)}}{\left(1+e^{-(w_i\eta+b_i)}\right)^2}\right), \tag{11}$$

will give ANN based governing equation of heat transfer. The ANN strategy and parameters such as input, hidden layer, and output are given in Figure 2.

IV. DESIGNING FITNESS FUNCTION

For quantitative evaluation of approximated solution fitness function is designed based on two mean-square errors, it's as follows::

$$min\quad E=E_1+E_2, \tag{12}$$

here E_1 denote the cost function, can be expressed as follows:

$$\begin{aligned}E_1&=\frac{1}{N}\sum_{m=1}^{N}\left(\frac{\mathrm{d}}{\mathrm{d}\eta}\left[\left(1+\varepsilon_1\hat{\theta}_m\right)\frac{\mathrm{d}\hat{\theta}_m}{\mathrm{d}\eta}\right]-\nu^2\hat{\theta}_m-\varepsilon_2\hat{\theta}_m^4\right)^2,\\ N&=\frac{1}{h},\quad \hat{g}_m=\hat{g}\left(\eta_m\right),\quad \eta_m=\mathrm{mh},\end{aligned} \tag{13}$$

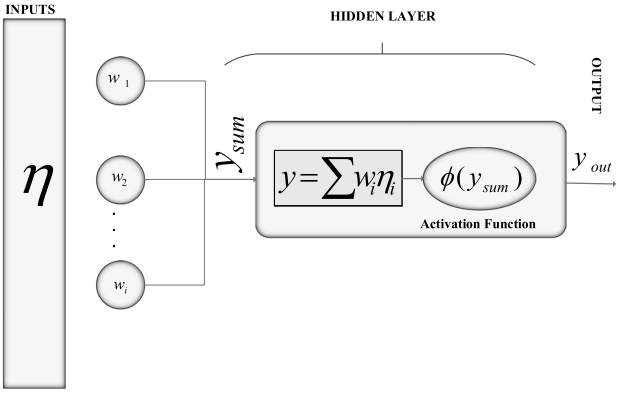

FIGURE 2. Working steps of artificial neural network.

where N denotes points the input points in the grid, the number of inputs depend on step size h in given interval, $\hat{\theta}(\eta)$, $\hat{\theta}'(\eta)$, and $\hat{\theta}''$ are given in equation (8). In similar manner, E_2 is the error in boundary conditions define as:

$$E_2 = \frac{1}{2}\left(\left(\frac{\mathrm{d}\hat{\theta}}{\mathrm{d}\eta}(0) - 0\right)^2 + \left(\hat{\theta}(1) - 1\right)^2\right). \tag{14}$$

The fitness value depends on the provision of neurons, $\mathbf{W} = [\mathbf{a}, \quad \mathbf{w}, \quad \zeta]$, the set of best neurons will tends the fitness value to zero. Which illustrate the minimum error in the approximated solution.

V. HYBRID TECHNIQUE FOR OPTIMIZATION PROCEDURE

A hybrid technique is adapted for the minimization of the fitness function define in equation (12). For this optimization procedure, two search strategies are used: global and local. For global performance, the Sine-Cosine algorithm (SCA) is used. The SCA was presented by Mirjalili [40]. Many further advancement are reported in literature such as crystal wave guides [41], for training of multi-layer perceptrons [42], unit commitment problem [43], and fuzzy probabilistic c-ordered means [44]. The SCA is inspired by trigonometric ratios Sine and Cosine. The mathematical strategy of SCA is as follows:

$$\begin{aligned} Y_i^{t+1} &= Y_i^t + r_1 \times \sin(r_2) \times \left|r_3 P_i^t - Y_i^t\right|, \\ Y_i^{t+1} &= Y_i^t + r_1 \times \cos(r_2) \times \left|r_3 P_l^t - Y_{ij}^t\right|, \end{aligned} \tag{15}$$

where Y_i represents the current location of the solution in the $i_t h$ dimension at the $t_t h$ iteration, $r_1/r_2/r_3$ are random quantities, P_i refers to the position of the target destination, and || represents absolute value. With parametric values, the equation (15) can be written as:

$$Y_l^{t+1} = \begin{cases} Y_i^t + r_1 \times \sin(r_2) \times \left|r_3 P_l^t - Y_i^t\right|, & r_4 < 0.5, \\ Y_l^t + r_1 \times \cos(r_2) \times \left|r_3 P_l^t - Y_{L_i}^t\right|, & r_4 \geq 0.5. \end{cases} \tag{16}$$

here r_4 is a random choice in the range [0,1]. There are four parameters in equation (16): r_1, r_2, r_3, and r_4. The direction of movement is indicated by the r_1, which could be within or outside of the feasible region. The r_2 parameter depicts the length from the region, as well as the direction toward or away from the target. The parameter r_3 represents target value weights, whereas r_4 operates equally the Sine and Cosine components of equation (16).

For the enhancement of local optimum performance of SCA, it is hybridized with Interior point algorithm (IPA). The IPA is an efficient technique for solving linear and non-linear optimization problems. The IPA is much better than trust regions and Sequential quadratic programming to solve the iterative problems [45]. The exploitation procedure of IPA refines the quality of solutions. The SCA is one of the population-based techniques which generates multiple solutions. As a starting point for IPA, the best solution is used. Later on in this work, the technique is abbreviated as ANN-SCA-IPA. The hybridization procedure is given in algorithm 1.

VI. PERFORMANCE MATRICES

Performance matrices are used to evaluate the effectiveness of the ANN—SCA—IPA approach. For relatable solutions the reliability and consistency of the proposed technique is necessary. For this purpose the performance measures Mean-absolute deviation (MAD), root-mean square error (RMSE), Nash–Sutcliffe efficiency (NSE) and error in Nash–Sutcliffe efficiency (ENSE). The definition of these performance matrices are as given:

$$MAD = \frac{1}{n}\sum_{i=1}^{n}\left|\theta(\eta_i) - \hat{\theta}(\eta_i)\right|, \tag{17}$$

$$RMSE = \sqrt{\frac{1}{n}\sum_{i=1}^{n}\left(\theta(\eta_i) - \hat{\theta}(\eta_i)\right)^2}, \tag{18}$$

$$NSE = 1 - \left(\frac{\sum_{i=1}^{n}\left(\theta(\eta_i) - \hat{\theta}(\eta_i)\right)^2}{\sum_{i=1}^{n}\left(\theta(\eta_i) - \frac{1}{n}\sum_{i=1}^{n}(\theta(\eta_i))\right)^2}\right), \tag{19}$$

$$ENSE = |1 - NSE|. \tag{20}$$

The set of input points in a grid is denoted by n, the proposed solution is $\hat{\theta}(\eta)$, and the reference solution is $\theta(\eta)$. The value of performance metrics MAD, ENSE, and RMSE should be approach zero for a dependable and effective system, whereas the NSE value tends to one.

The mathematical definition of the global version of the performance matrices stated above is define as:

$$GMAD = \frac{1}{R}\sum_{r=1}^{R}\left(\frac{1}{n}\sum_{i=1}^{n}\left(\left|\theta(\eta_i) - \hat{\theta}(\eta_i)\right|\right)\right), \tag{21}$$

Algorithm 1 Pseudocode of ANN-SCA-IPA Algorithm

Start: *Sine-Cosine Algorithm(SCA)*
Inputs:
Unknown Variable of ANN $W = [a, w, \zeta]$
Population size $P = [W_1, W_2, \ldots, W_m]^t = [(a_1, w_1, \zeta_1), (a_2, w_2, \zeta_2), \ldots, (a_m, w_m, \zeta_m)]^T$, *for* m *number of*
W *stands for weights in P, and*
t *denote transpose of vector* W ***Output:*** *Weights, with minimum objective value, of SCA, i-e.,* W_b
Begin
→ *Initialization*
Random generated real valued vector W *in a given span*
Set of m *weights vectors formulate the preliminary population* P.
// *Termination-Criteria (TC)*
Algorithm-TC → *if reach one of the given criteria:*
Fitness or Objective value → 10^{-16}.
Fun-Tol (Function Tolerance) → 10^{-20}
Con-Tol (Constrained Tolerance) → 10^{-20}.
Main-loop of SCA
While
If any one of Termination-Criteria satisfy
do
→ *Fitness-calculation*
Evaluate fitness function E given in Eq. (12) for the vector of weights W.
Repetition for m *weights W of the population* P.
→ *Check the achievement of TC*
If TC achieved, then exit the loop else repeat.
→ *Parameters of SCA*
Updating the population and check fitness valuse for each
End
→ ***Storing-Step***
Store: the vector as W_b *having minimum fitness value, function evaluation and time for the current run of the SCA.*
End SCA

Start IPA
→ *Initialization of IPA*
Initializing IPA technique with best weights vector W_b *of SCA as an initial guess vector.*
Set the Termination-criteria TC:
Max-Iter (Maximum-iterations), i.e. 1000,
Fun-Tol as 10^{-24}
Con-Tol as 10^{-24} *and*
Tolerance in optimization variables(weights), i.e., Tol-X as 10^{-16},
While
any of TC Value achieved do
→ *Next step: Fitness Evaluation*
Evaluate E values as in Eq. (12) for the vector.
→ *Test for TC*
If TC achieved, then terminate the loop else repeat.
→ *Updating step*
Set 'fmincon' function with method 'Interior-point algorithm'
Update weight-vector for each step through IPA-optimization procedure.
Repeat procedure till the achievement of desired fitness
→ *Storing-step*
Store: the final weight-vector having minimum fitness value, time,
function evaluation, and generation consumed for the SCA-IPA method.
End IPA
Evaluation: *Execute the mechanism of SCA-IPA for 100 independent runs*
to generate sufficient set of data for effective and reliable performance evaluation of ANN-SCA-IPA.

$$GRMSE = \frac{1}{R}\sum_{r=1}^{R}\left(\sqrt{\frac{1}{n}\sum_{i=1}^{n}\left(\theta(\eta_i) - \hat{\theta}(\eta_i)\right)^2}\right), \tag{22}$$

$$GENSE = \frac{1}{R}\sum_{r=1}^{R}\left(\frac{\sum_{i=1}^{n}\left(\theta(\eta_i) - \hat{\theta}(\eta_i)\right)^2}{\sum_{i=1}^{n}\left(\theta(\eta_i) - \frac{1}{n}\sum_{i=1}^{n}(\theta(\eta_i))\right)}\right), \tag{23}$$

$$GFIT = \frac{1}{R}\sum_{r=1}^{R}E_r, \tag{24}$$

where, R denotes the number of multiple independent runs, and E_r denotes the fitness value of the ANN—SCA—IPA at r_th number run. All global operators have a standard or optimum value of zero. The global version is based on the mean fitness value. Global operators are abbreviated as: GFIT for fitness, GMAD for MAD, GRMSE for RMSE and, GENSE for ENSE.

VII. EMPIRICAL RESULTS AND DISCUSSION

This section discusses the outcome of dynamics of heat transfer, given in equation (5). The heat transfer problem's dynamics are described on variation of thermal conductivity, thermal convection, and radiation with different temperature distributions. The dynamics are quantitatively executed by ANN-SCA-IPA algorithm. Moreover, the discussion is split into four examples.

A. EXAMPLE 1: CONDUCTIVE HEAT TRANSFER

In this example, the heat transfer is considered only through conduction, ϵ_1. There is no heat transfer by convection ($\nu = 0$) and radiation ($\epsilon_2 = 0$). The example has three cases, in Case I is consider as $\epsilon_1 = 0.1$, for

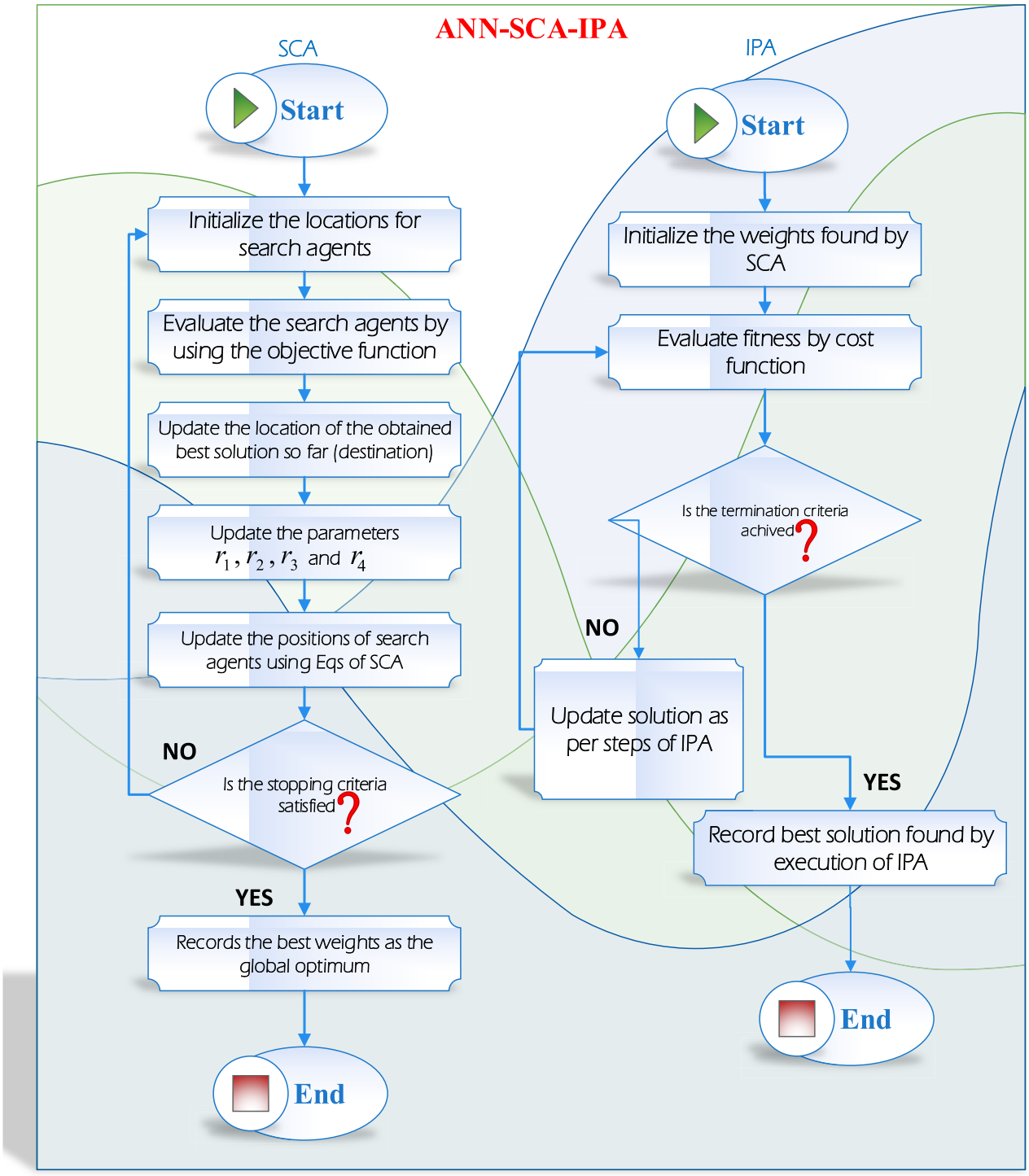

FIGURE 3. Blocks chart of ANN-SCA-IPA.

case II $\epsilon_1 = 0.6$ and for case III $\epsilon_1 = 0.9$. The in put point is taken in [0, 1], so for N input points the fitness function given in equations (12)-(14) can updated as:

$$E_{cI} = \frac{1}{N}\sum_{m=1}^{N}\left(\frac{\mathrm{d}}{\mathrm{d}\eta}\left[\left(1+0.1\hat{\theta}_m\right)\frac{\mathrm{d}\hat{\theta}_m}{\mathrm{d}\eta}\right] - \nu^2\hat{\theta}_m - \varepsilon_2\hat{\theta}_m^4\right)^2 + \frac{1}{2}\left(\left(\hat{\theta}(0)-1\right)^2 + \left(\hat{\theta}(1)\right)^2\right), \tag{25}$$

$$E_{cII} = \frac{1}{N}\sum_{m=1}^{N}\left(\frac{\mathrm{d}}{\mathrm{d}\eta}\left[\left(1+0.6\hat{\theta}_m\right)\frac{\mathrm{d}\hat{\theta}_m}{\mathrm{d}\eta}\right] - \nu^2\hat{\theta}_m - \varepsilon_2\hat{\theta}_m^4\right)^2 + \frac{1}{2}\left(\left(\hat{\theta}(0)-1\right)^2 + \left(\hat{\theta}(1)\right)^2\right), \tag{26}$$

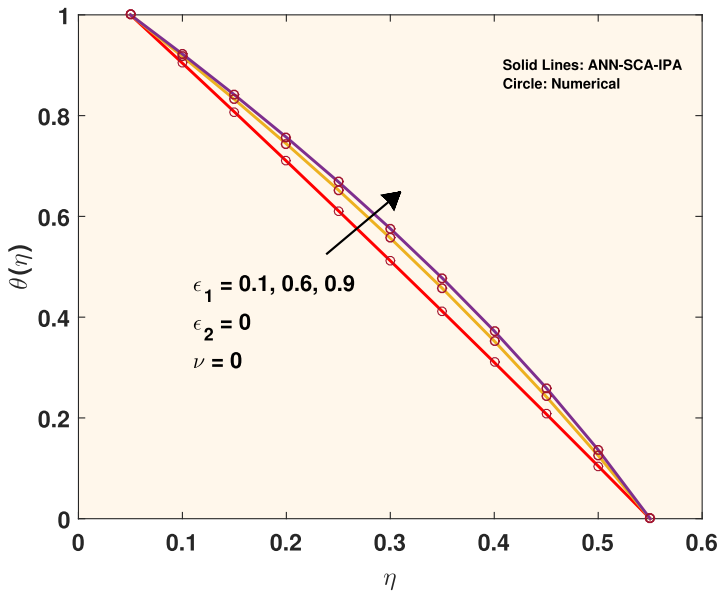

(a) Solution of Example I for $\epsilon_1 = 0.1, 0.6, 0.9, and \epsilon_2 = \nu = 0$

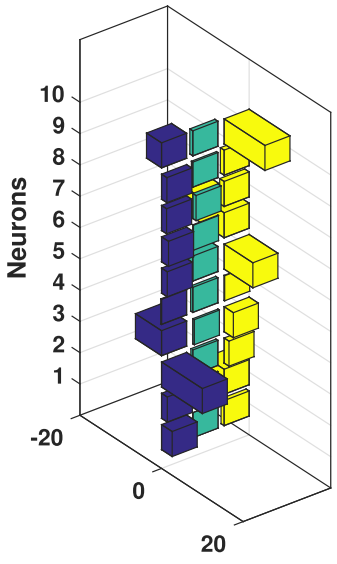

(b) Weights for $\epsilon_1 = 0.1$

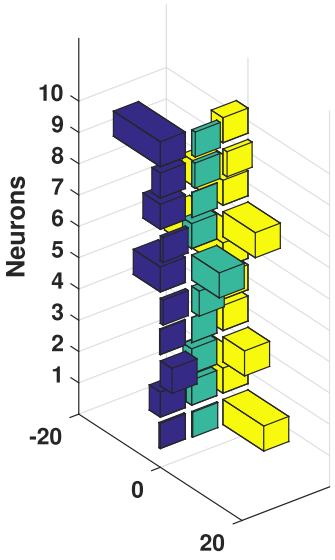

(c) Weights for $\epsilon_1 = 0.6$

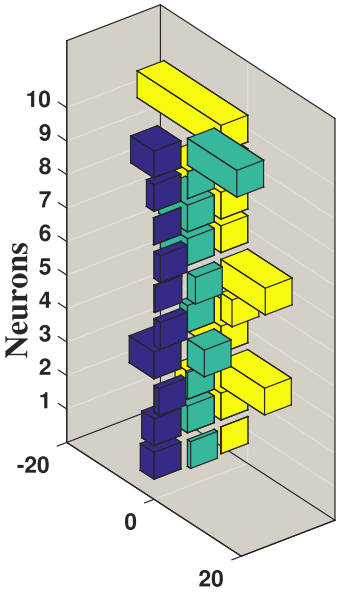

(d) Weights for $\epsilon_1 = 0.9$

FIGURE 4. **(a) Example 1: Shows graph of conductive heat transfer, (b-d) is 3D bar graph of weights obtain by ANN-SCA-IPA algorithm.**

$$E_{cIII} = \frac{1}{N}\sum_{m=1}^{N}\left(\frac{\mathrm{d}}{\mathrm{d}\eta}\left[\left(1+0.9\hat{\theta}_m\right)\frac{\mathrm{d}\hat{\theta}_m}{\mathrm{d}\eta}\right] - v^2\hat{\theta}_m - \varepsilon_2\hat{\theta}_m^4\right)^2 + \frac{1}{2}\left(\left(\hat{\theta}(0)-1\right)^2 + \left(\hat{\theta}(1)\right)^2\right),, \tag{27}$$

as the minimization is done by ANN-SCA-IPA algorithm for the solution of this example with minimum errors. The best unknown variable called weights of ANN is plugged in equation (9) to get the solution. For the set of appropriate weights, 30 neurons are considered. The solution for each case is given as:

$$\hat{\theta}_{cI}(\eta) = \frac{2.6026264251}{1+\mathrm{e}^{-(0.0170122659\eta-0.7547085701)}} + \cdots + \frac{-3.6918806682}{1+\mathrm{e}^{-(-0.7415670806\eta+10.0049716432)}}, \tag{28}$$
$$\hat{\theta}_{cII}(\eta) = \frac{-0.35794133146}{1+\mathrm{e}^{-(0.26391440801\eta+9.99975372453)}} + \cdots$$

TABLE 1. Appropriate weights for Example I.

	Case I			Case II			Case III		
i	a_i	w_i	ζ_i	a_i	w_i	ζ_i	a_i	w_i	ζ_i
1	2.602626425199950	0.017012265990431	-0.754708570112332	-0.357941331469442	0.263914408013947	9.999753724537010	-3.160030421256840	0.731763670921144	0.045763631312986
2	1.410326813508950	-0.106063731378422	-4.508911917589510	-2.724065933480070	-1.303765203203730	-9.704621404687740	-2.829468217350180	-2.330217925806630	-10.505640512331300
3	9.991301864537020	-0.488942546889799	1.193186518993810	2.858335716142380	-2.124441556405070	5.296412017375190	1.128868981335700	-0.430490462257322	10.001178949648800
4	-6.401536261568260	0.373978998229374	2.263369191898170	-0.199378518773686	0.004377735420499	-1.796774245501330	-5.696743625863290	3.859346773727500	-7.882820188294610
5	-0.199172829074871	-0.535537746258558	0.139462002950955	0.714630219514311	1.854457991447940	-2.907284168359370	1.457756257111440	-1.743111789631680	2.537677158363040
6	1.398017949953400	-1.741125501404640	7.045511245877330	-6.643245793486100	6.757331730201840	-14.318697811704400	0.253098599380301	1.822910716480460	10.158826792544700
7	1.708310396440250	0.156820720913337	-10.000149875877400	0.659072044701326	-2.243884577467410	7.931432902689700	1.441895148363780	-6.197686079654040	-9.618458024062980
8	1.235687488216280	0.785900783916801	-1.083496764304090	-4.274948158572280	0.102041701845941	-9.999498871372750	-0.137359755994750	-6.584774430226550	-13.428808749920200
9	1.310664872117550	-0.352371709696856	-0.920640239999641	-2.082388884863260	0.798661535406449	1.016277768335630	-1.744131129540340	0.038685315822426	-2.654810962710240
10	-3.691880668283030	-0.741567080633551	10.004971643282500	-11.514052617624300	0.884875618136333	-2.858946319922500	-5.358670946408050	11.309488297483300	-19.204188936269600

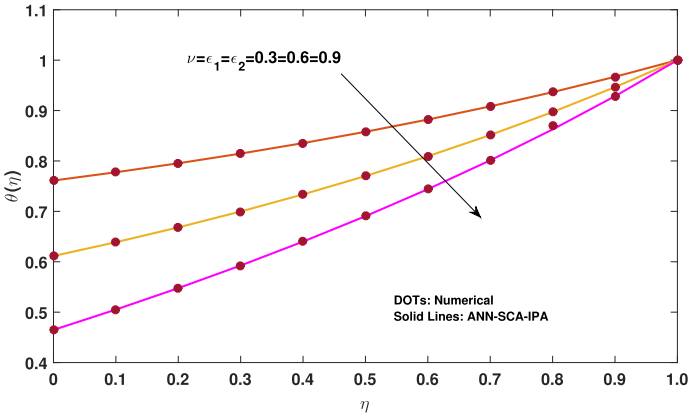

(a) Solution of Example II for $\epsilon_1 = \epsilon_2 = \nu = 0.3,\ 0.6,\ 0.9$

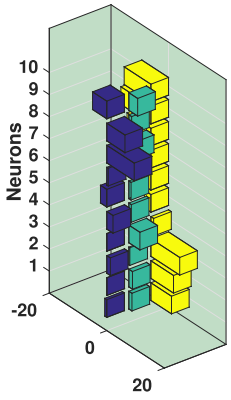

(b) Weights for $\epsilon_1 = \epsilon_2 = \nu = 0.3$

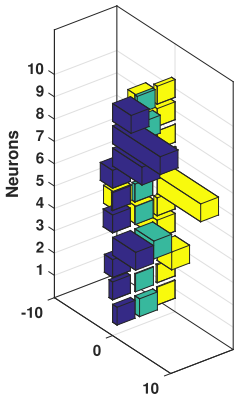

(c) Weights for $\epsilon_1 = \epsilon_2 = \nu = 0\ 6$

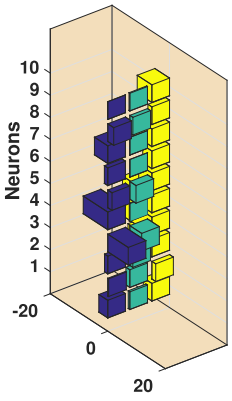

(d) Weights for $\epsilon_1 = \epsilon_2 = \nu = 0\ 9$

FIGURE 5. (a) Example 2: Shows graph of heat transfer at same rate, (b-d) is 3D bar graph of weights obtain by ANN-SCA-IPA algorithm.

$$+\frac{-11.51405261762}{1+\mathrm{e}^{-(0.88487561813\eta-2.85894631992)}}, \quad (29)$$

$$\hat{\theta}_{cIII}(\eta) = \frac{-3.16003042125}{1+\mathrm{e}^{-(0.73176367092\eta+0.04576363131)}} + \cdots$$

$$+\frac{-5.35867094640}{1+\mathrm{e}^{-(11.30948829748\eta-19.2041889362)}}, \quad (30)$$

the full form of equations (28)–(30) is given in the Appendix for up to 14-decimal places. The approximated solutions are graphically compared with the solution of Runge–Kutta order 4 (RK4) shown in Figure 4a. The solution is plotted with step size 0.1 in the interval [0, 1]. The weights are also drawn with 3D bar graphs in figure 4(b–c). The weights are also reported in table 1. The dots (·) show the results of RK4, and the solid lines represent approximated solutions. The overlapping of these solutions shows the convergence of ANN-SCA-IPA algorithm.

TABLE 2. Appropriate weights for Example II.

	Case I			Case II			Case III		
i	a_i	w_i	ζ_i	a_i	w_i	ζ_i	a_i	w_i	ζ_i
1	-0.72209177714401	1.08534561843429	7.16771353183543	0.77562319275331	0.80312814366847	-0.11481120910708	-3.11166311355570	-0.55862057469788	-3.00080260714515
2	0.04280795866075	1.26062518486213	7.86840631849982	-0.62067093754196	0.11902594229190	-0.20135934162277	0.30305798014334	-1.35647289401072	1.33621293321447
3	1.23961571072966	0.34786678079970	10.02771130087240	-1.41185838119190	-0.84941273573146	2.49804893280840	-1.13746906171566	1.04092318554189	-8.31654930576994
4	-0.00179796402332	3.84818477203120	0.96129887186568	3.96807434923300	3.24816241881950	-9.22361453088584	7.11169711801073	4.12180683552389	-10.78234970096540
5	2.15937416561598	0.86794706218372	-2.25376234192617	-1.61648970252284	0.05614251411021	-0.57504533451014	-8.54544710025029	-0.19712305524108	-10.23471022436020
6	-2.19668605661773	0.77907794181637	-5.86236139355454	-0.19245297838728	-0.48130629175333	7.47785775594154	1.46907030267998	2.14061929930493	-4.57944733461099
7	0.51218207630391	-3.45574574816393	-6.74718236894939	-2.11629887651201	-0.26947771644126	0.16310691037096	-1.19394658008619	-0.00415777540841	-3.18222939953020
8	9.53949707835880	2.60633991229409	-8.29571411372836	5.05002527130982	-0.35263596200807	0.01858350694855	-4.64143187858800	-0.03501709929709	-6.32984963876366
9	6.31984108175878	0.97837527177603	-10.43419369747310	8.17811790758776	1.28811672644753	-5.05091171238374	2.06261605537133	1.05804115940204	-1.38186954787184
10	-4.95239845098011	3.07259650250602	-9.28938641662133	3.18573685425379	0.40744662084733	-0.57466218873775	-0.06157136406944	-0.28839239020430	-5.09784089449052

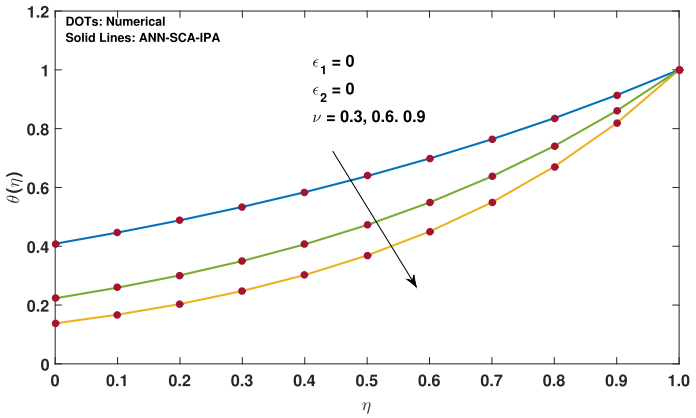

(a) Solution of Example 3 for $\epsilon_1 = \epsilon_2 = 0, \nu = 0.3,\ 0.6,\ 0.9$

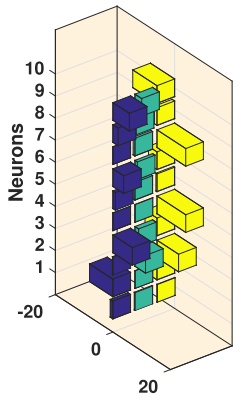

(b) Weights for $\nu = 0.3$

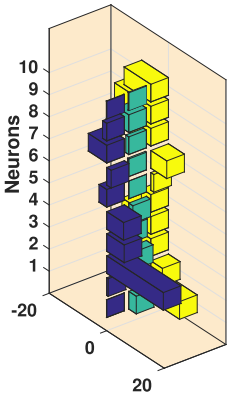

(c) Weights for $\nu = 0.6$

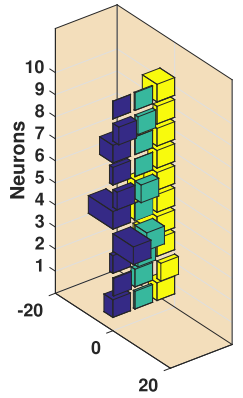

(d) Weights for $\nu = 0.9$

FIGURE 6. (a) Example 3: Shows graph of convective heat transfer, (b-d) is 3D bar graph of weights obtain by ANN-SCA-IPA algorithm.

TABLE 3. Appropriate weights for Example 3.

	Case I			Case II			Case III		
i	a_i	w_i	ζ_i	a_i	w_i	ζ_i	a_i	w_i	ζ_i
1	-1.01185927939554	-0.55657898918396	-8.24367836630025	-0.07826822263912	2.61043704472045	10.00495723288270	-1.01185927939554	-0.55657898918396	-8.24367836630025
2	0.42332346768074	1.04818888954528	6.24199946450650	0.52328826967484	-1.61540136515781	4.03035047431375	0.42332346768074	1.04818888954528	6.24199946450650
3	-1.25804705230632	-0.01996137340253	0.61808094535690	19.69137465607900	2.30756824211167	-6.63552225203931	-1.25804705230632	-0.01996137340253	0.61808094535690
4	1.40028536283575	-2.29555729756490	-6.80851182008727	6.07294531961497	0.31023395404365	-10.04850064355280	1.40028536283575	-2.29555729756490	-6.80851182008727
5	-0.41531435170868	0.27350533962287	1.98056422786804	5.87087161880098	1.42942155709545	-3.28117991162135	-0.41531435170868	0.27350533962287	1.98056422786804
6	82.63131929346360	2.29565376715677	-7.06108361272853	-2.70149977820962	0.00106561447786	1.03603182918973	82.63131929346360	2.29565376715677	-7.06108361272853
7	1.53836443437645	1.66662137598802	-3.04642381749867	1.54829550159043	-0.42453959955613	5.54963527031857	1.53836443437645	1.66662137598802	-3.04642381749867
8	3.15068685470091	0.60211099381737	-7.48364468091623	-6.41292444801804	-1.04739573280067	-12.54980321255120	3.15068685470091	0.60211099381737	-7.48364468091623
9	7.59607658451329	19.53251090294720	-45.96246020569060	-1.44420074640622	-4.08652035246089	-12.61667769048580	7.59607658451329	19.53251090294720	-45.96246020569060
10	0.75418971607839	0.46245191385923	8.01705218107347	-0.15128880482211	-0.25175398302269	-9.29117452182819	0.75418971607839	0.46245191385923	8.01705218107347

B. EXAMPLE 2: HEAT TRANSFER WITH CONSTANT RATE

In this example, the heat transfer is consider through conduction (ϵ_1), convection (ν) and radiation (ϵ_2) with a same rate. The rate of heat transfer is discussed in three cases. In Case I, the rate is considered 0.3, in case II 0.6, and case III 0.9. The input points are taken in [0, 1], so for N input points

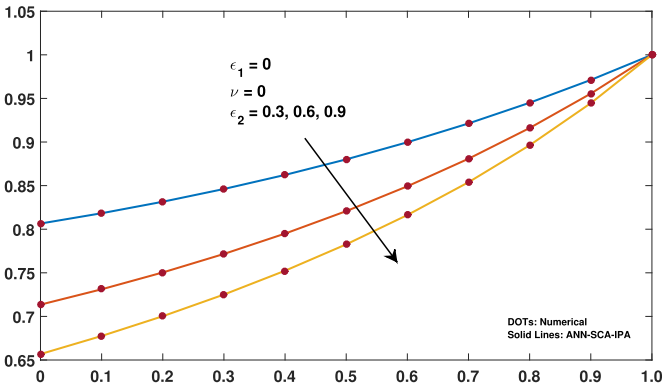

(a) Solution of Example 1 for $\epsilon_1 = \nu = 0, \epsilon_2 = 0.3,\ 0.6,\ 0.9$

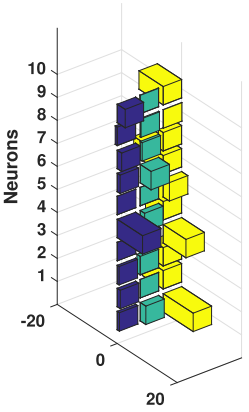

(b) Weights for $\epsilon_2 = 0.3$

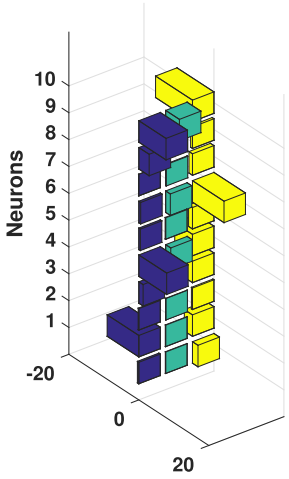

(c) Weights for $\epsilon_2 = 0.6$

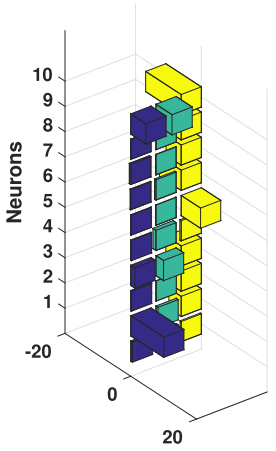

(d) Weights for $\epsilon_2 = 0.9$

FIGURE 7. (a) Example 4: Shows graph of radiative heat transfer, (b-d) is 3D bar graph of weights obtain by ANN-SCA-IPA algorithm.

TABLE 4. Appropriate weights for Example 4.

	Case I			Case II			Case III		
i	a_i	w_i	ζ_i	a_i	w_i	ζ_i	a_i	w_i	ζ_i
1	0.74062602589450	1.88116069135493	10.00096346483250	-0.41305077146786	-0.09739961021451	1.57631121828062	0.51592740916267	0.59151605350915	-0.34362355396436
2	1.03663095336656	0.00232129409015	-6.92575655577716	-9.06168775198311	-0.10439293579204	-2.33285595069587	10.04875321976760	0.63359216910404	-3.73919912955813
3	0.63870129027722	-1.10154546020021	-3.82280135108194	-0.19415976312872	0.07704054432782	-0.30831610677716	0.24973432659304	0.03888987491724	-3.43884480748675
4	0.07872804882445	0.64711489929556	7.58682879526516	1.21977781626752	-0.66840966813709	-1.77230767875457	1.26031300226193	2.29973485022297	-4.64649613543273
5	8.449640211933396	1.47821204704096	-5.89897467946119	7.95475137561544	1.45638288665383	-5.07000888295891	0.21824990580200	-0.92313923728472	-0.41280136055752
6	0.04564482364660	-0.02489304677948	2.07694476281271	0.44530897708341	-0.14896338181865	-1.12104793020020	0.10756961172771	-0.09584042832107	5.90053019606209
7	0.97943273956507	3.60979070588798	-9.83688301821155	0.53027328731519	1.33265178057718	9.00964702012568	-0.22133826297203	-0.43428097122780	-6.60047115445034
8	1.48756192699492	0.65635482762209	-1.55106167211939	-0.07714631360615	0.18434800984411	-0.99750720145526	-0.46333688215918	-0.13462066365561	-4.60227347725252
9	-0.67466483472825	0.28787235529010	0.08842270466001	2.95043827160706	0.19351302714722	-0.52955888693544	0.00674907224545	0.00135428870559	-3.29806758291949
10	2.67237229127701	-0.12625759873150	-8.08334676618897	7.76832664863492	3.93224162230843	-10.55871354144050	4.62704335160515	4.89230523280703	-10.79973815336560

the fitness function given in equations (12)-(14) can updated as:

$$E_{c1} = \frac{1}{N}\sum_{m=1}^{N}\left(\frac{\mathrm{d}}{\mathrm{d}\eta}\left[\left(1+0.3\hat{\theta}_m\right)\frac{\mathrm{d}\hat{\theta}_m}{\mathrm{d}\eta}\right]-0.3^2\hat{\theta}_m - 0.3\hat{\theta}_m^4\right)^2 + \frac{1}{2}\left(\left(\frac{\mathrm{d}\hat{\theta}}{\mathrm{d}\eta}(0)\right)^2+\left(\hat{\theta}(1)-1\right)^2\right), \tag{31}$$

$$E_{c2} = \frac{1}{N}\sum_{m=1}^{N}\left(\frac{\mathrm{d}}{\mathrm{d}\eta}\left[\left(1+\varepsilon_1\hat{\theta}_m\right)\frac{\mathrm{d}\hat{\theta}_m}{\mathrm{d}\eta}\right]-\nu^2\hat{\theta}_m - \varepsilon_2\hat{\theta}_m^4\right)^2 + \frac{1}{2}\left(\left(\frac{\mathrm{d}\hat{\theta}}{\mathrm{d}\eta}(0)\right)^2+\left(\hat{\theta}(1)-1\right)^2\right),, \tag{32}$$

$$E_{c3} = \frac{1}{N}\sum_{m=1}^{N}\left(\frac{\mathrm{d}}{\mathrm{d}\eta}\left[\left(1+\varepsilon_1\hat{\theta}_m\right)\frac{\mathrm{d}\hat{\theta}_m}{\mathrm{d}\eta}\right]-\nu^2\hat{\theta}_m - \varepsilon_2\hat{\theta}_m^4\right)^2$$

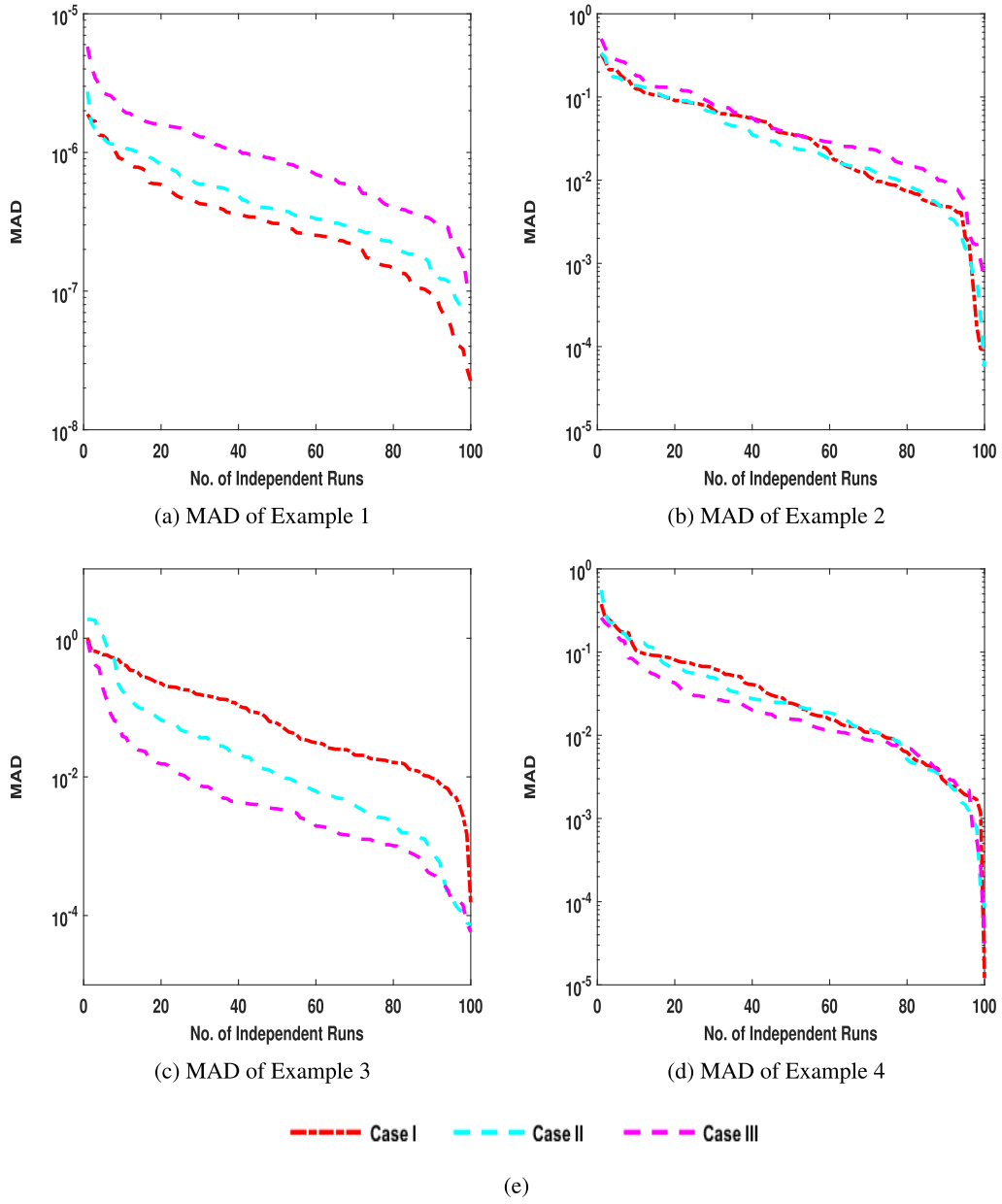

(a) MAD of Example 1

(b) MAD of Example 2

(c) MAD of Example 3

(d) MAD of Example 4

(e)

FIGURE 8. **(a–d) show data of performance operator MAD, the data of 100 independent runs is sorted in descending order, having a log along the *y*-axis.**

$$+\frac{1}{2}\left(\left(\frac{\mathrm{d}\hat{\theta}}{\mathrm{d}\eta}(0)\right)^2+\left(\hat{\theta}(1)-1\right)^2\right), \tag{33}$$

as the minimization is done by ANN-SCA-IPA algorithm for the solution of this example with minimum errors. The best unknown variable called weights of ANN found is plugged in equation (9) to get the solution. For the set of appropriate weights, 30 neurons are considered. The solution for each case is given as:

$$\hat{\theta}_{cI}(\eta)=\frac{-0.72209177714}{1+\mathrm{e}^{-(1.08534561843\eta+7.16771353183)}}+\cdots$$

$$+\frac{-4.95239845098}{1+\mathrm{e}^{-(3.07259650250\eta-9.28938641662)}}, \tag{34}$$

$$\hat{\theta}_{cII}(\eta)=\frac{0.77562319275}{1+\mathrm{e}^{-(0.80312814366\eta-0.11481120910)}}+\cdots$$

$$+\frac{-4.95239845098}{1+\mathrm{e}^{-(3.07259650250\eta-9.28938641662)}}, \tag{35}$$

$$\hat{\theta}_{cIII}(\eta)=\frac{-3.1116631135}{1+\mathrm{e}^{-(-0.5586205746\eta-3.0008026071)}}+\cdots$$

$$+\frac{-0.0615713640}{1+\mathrm{e}^{-(-0.2883923902\eta-5.0978408944)}}, \tag{36}$$

the full form of Equations (34)–(36) is given in the Appendix for up to 14-decimal places. The approximated solutions

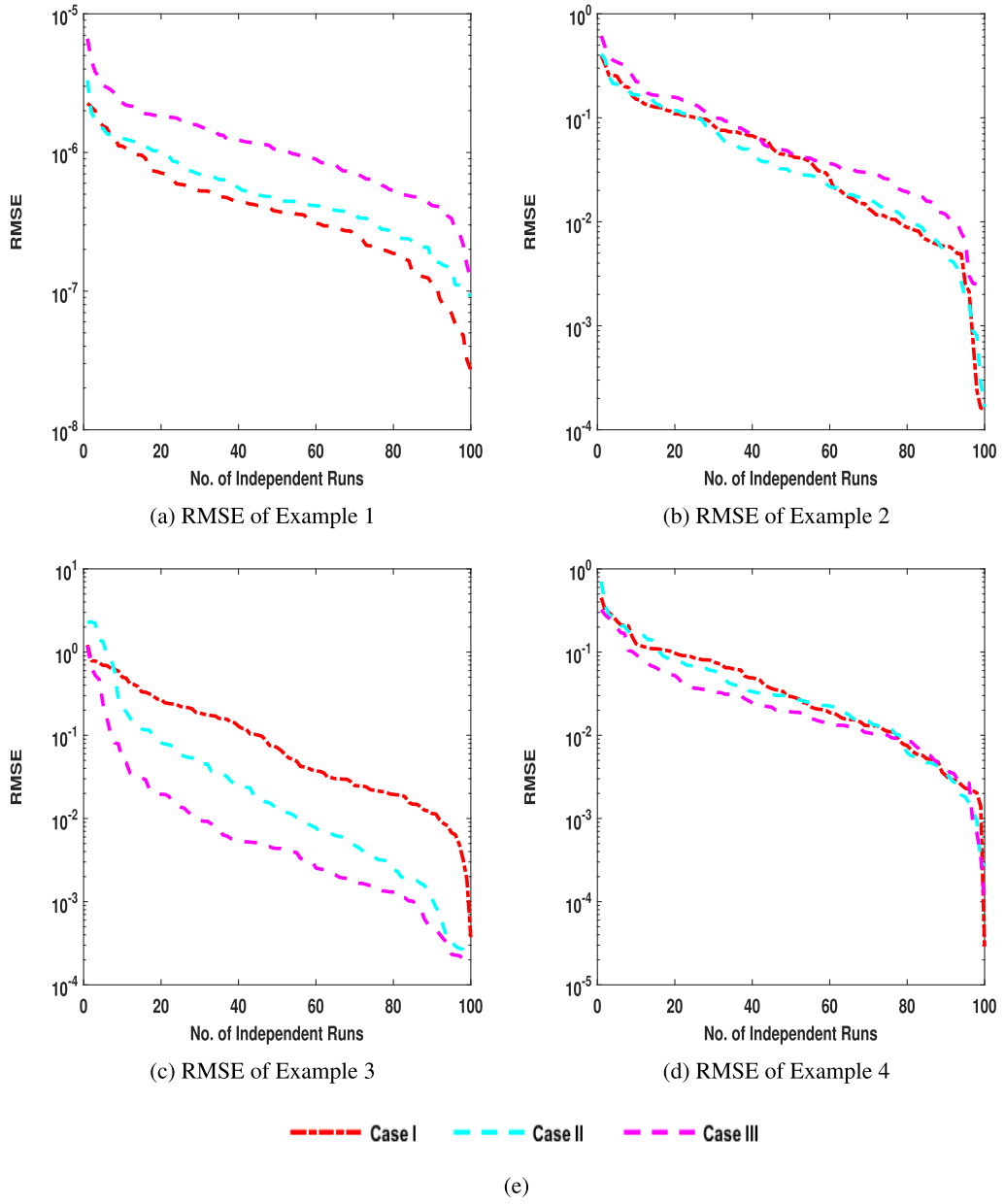

(a) RMSE of Example 1

(b) RMSE of Example 2

(c) RMSE of Example 3

(d) RMSE of Example 4

(e)

FIGURE 9. (a–d) show data of performance operator RMSE, the data of 100 independent runs is sorted in descending order, having a log along the *y*-axis.

are graphically compared with the solution of Runge–Kutta order 4 (RK4) shown in Figure 5a. The solution is plotted with step size 0.1 in the interval [0, 1]. The weights are also drawn with 3D bar graphs in figure 5(b–c). The weights are also reported in table 2. The dots (·) show the results of RK4, and the solid lines represent approximated solutions. The overlapping of these solutions shows the convergence of ANN-SCA-IPA algorithm.

C. EXAMPLE 3: CONVECTIVE HEAT TRANSFER

In this example, the heat transfer is consider through convection, ν, only. There is no heat transfer by conduction ($\epsilon_1 = 0$) and radiation ($\epsilon_2 = 0$). The example has three cases, in Case I convection consider as $\nu = 0.3$, for case II $\nu = 0.6$ and for case III $\nu = 0.9$. The in put point is taken in [0, 1], so for N input points the fitness function given in equations (12)-(14) can updated as:

$$_{c1} = \frac{1}{N}\sum_{m=1}^{N}\left(\frac{\mathrm{d}}{\mathrm{d}\eta}\left[\left(1+\varepsilon_1\hat{\theta}_m\right)\frac{\mathrm{d}\hat{\theta}_m}{\mathrm{d}\eta}\right] - 0.3^2\hat{\theta}_m - \varepsilon_2\hat{\theta}_m^4\right)^2 + \frac{1}{2}\left(\left(\frac{\mathrm{d}\hat{\theta}}{\mathrm{d}\eta}(0)\right)^2 + \left(\hat{\theta}(1)-1\right)^2\right), \tag{37}$$

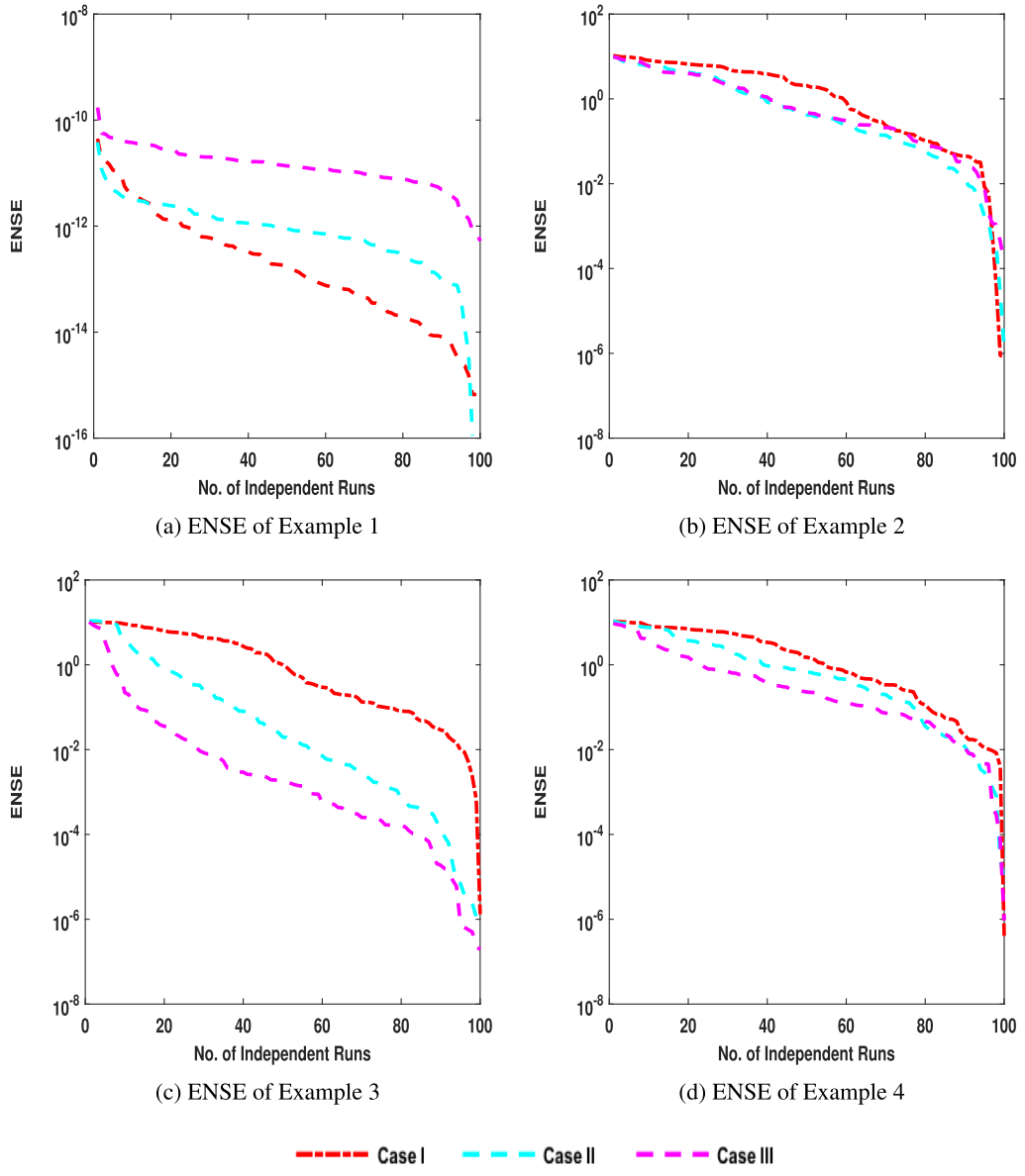

(a) ENSE of Example 1

(b) ENSE of Example 2

(c) ENSE of Example 3

(d) ENSE of Example 4

(e)

FIGURE 10. **(a–d) show data of performance operator ENSE, the data of 100 independent runs is sorted in descending order, having a log along the *y*-axis.**

$$E_{c2} = \frac{1}{N}\sum_{m=1}^{N}\left(\frac{\mathrm{d}}{\mathrm{d}\eta}\left[\left(1+\varepsilon_1\hat{\theta}_m\right)\frac{\mathrm{d}\hat{\theta}_m}{\mathrm{d}\eta}\right] - 0.3^2\hat{\theta}_m - \varepsilon_2\hat{\theta}_m^4\right)^2 + \frac{1}{2}\left(\left(\frac{\mathrm{d}\hat{\theta}}{\mathrm{d}\eta}(0)\right)^2 + \left(\hat{\theta}(1)-1\right)^2\right), \tag{38}$$

$$E_{c3} = \frac{1}{N}\sum_{m=1}^{N}\left(\frac{\mathrm{d}}{\mathrm{d}\eta}\left[\left(1+\varepsilon_1\hat{\theta}_m\right)\frac{\mathrm{d}\hat{\theta}_m}{\mathrm{d}\eta}\right] - 0.9^2\hat{\theta}_m - \varepsilon_2\hat{\theta}_m^4\right)^2 + \frac{1}{2}\left(\left(\frac{\mathrm{d}\hat{\theta}}{\mathrm{d}\eta}(0)\right)^2 + \left(\hat{\theta}(1)-1\right)^2\right), \tag{39}$$

as the minimization is done by ANN-SCA-IPA algorithm for the solution of this example with minimum errors. The best unknown variable called weights of ANN found is plugged in equation (9) to get the solution. For the set of appropriate weights, 30 neurons are considered. The solution for each case is given as:

$$\hat{\theta}_{cI}(\eta) = \frac{-0.72209177714}{1+\mathrm{e}^{-(1.08534561843\eta+7.16771353183)}} + \cdots + \frac{-4.95239845098}{1+\mathrm{e}^{-(3.07259650250\eta-9.28938641662)}}, \tag{40}$$

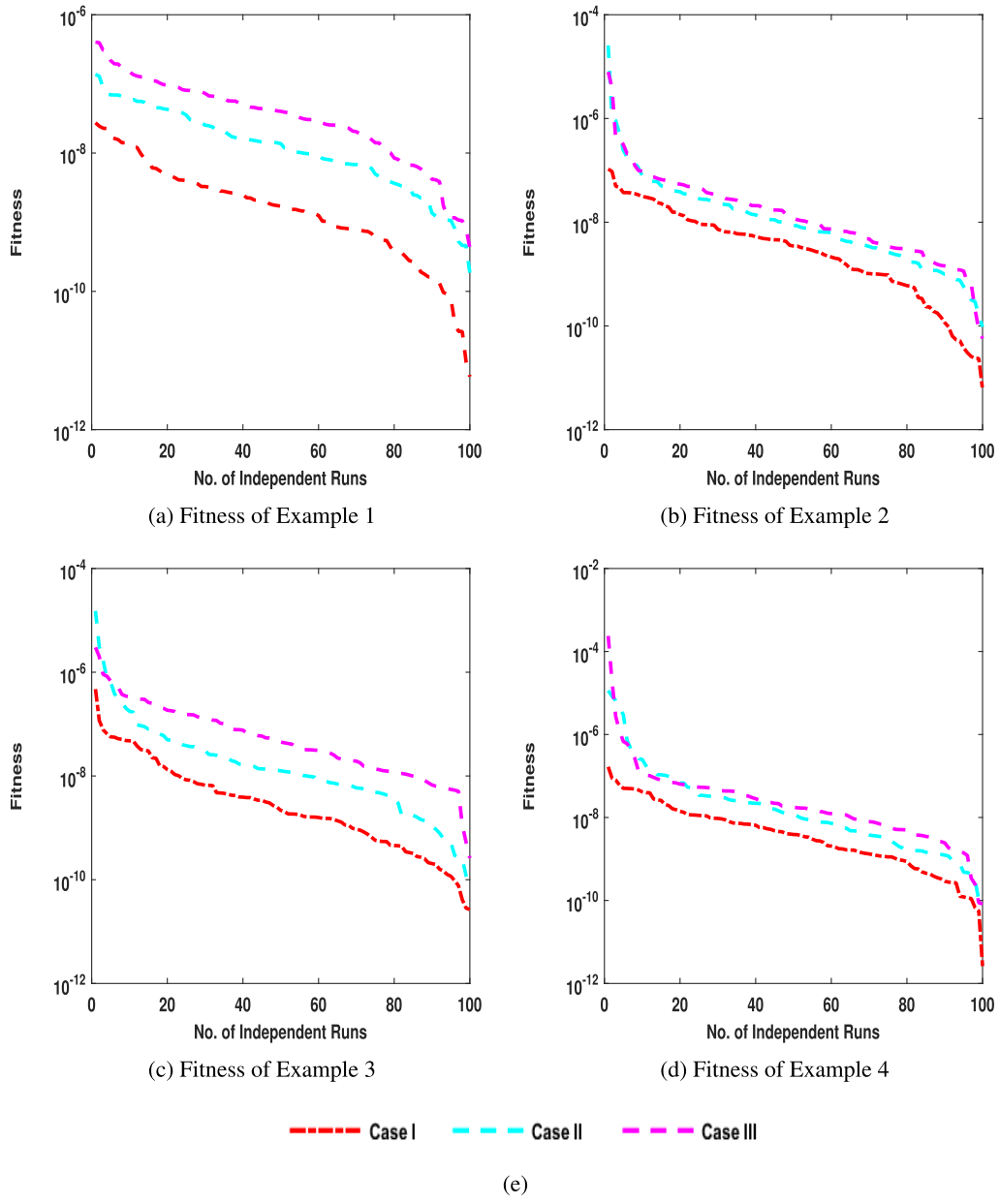

(a) Fitness of Example 1
(b) Fitness of Example 2
(c) Fitness of Example 3
(d) Fitness of Example 4
(e)

FIGURE 11. (a–d) show data of fitness, the data of 100 independent runs is sorted in descending order, having a log along the *y*-axis.

$$\hat{\theta}_{cII} = \frac{-0.078268222639117}{1+\mathrm{e}^{-(2.610437044720450\eta+10.004957232882700)}} + \cdots + \frac{-0.151288804822108}{1+\mathrm{e}^{-(-0.251753983022694\eta-9.291174521828190)}}, \tag{41}$$

$$\hat{\theta}_{cIII} = \frac{-1.011859279395540}{1+\mathrm{e}^{-(-0.556578989183962\eta-8.243678366300250)}} + \cdots + \frac{0.754189716078391}{1+\mathrm{e}^{-(0.462451913859229\eta+8.017052181073470)}}, \tag{42}$$

the full form of Equations (40)–(42) is given in the Appendix for up to 14-decimal places. The approximated solutions are graphically compared with the solution of Runge–Kutta order 4 (RK4) shown in Figure 6a. The solution is plotted with step size 0.1 in the interval [0, 1]. The weights are also drawn with 3D bar graphs in figure 6(b–c). The weights are also reported in table 3. The dots (·) show the results of RK4, and the solid lines represent approximated solutions. The overlapping of these solutions shows the convergence of ANN-SCA-IPA algorithm.

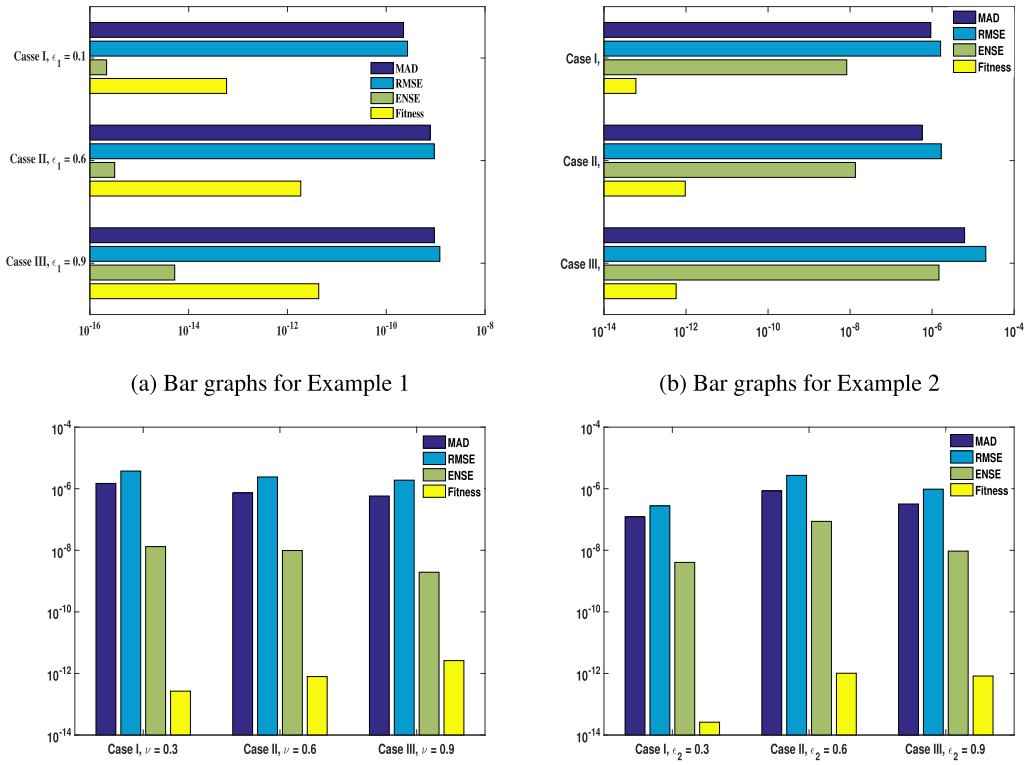

(a) Bar graphs for Example 1

(b) Bar graphs for Example 2

(c) Bar graphs for Example 3

(d) Bar graphs for Example 4

FIGURE 12. (a–d) shows minimum value of MAD, RMSE, ENSE and fitness with the help of bar graph.

TABLE 5. Quantitative evaluation by global performance operators.

Example	Case	GMAD	GRMSE	GENSE	GFIT
	I	2.24×10^{-10}	2.70×10^{-10}	1.44×10^{-16}	5.85×10^{-14}
1	II	7.79×10^{-10}	$9.3i7\times10^{-10}$	3.35×10^{-16}	1.86×10^{-12}
	III	9.45×10^{-10}	1.22×10^{-09}	5.22×10^{-15}	4.30×10^{-12}
	I	9.29×10^{-07}	1.61×10^{-06}	8.30×10^{-09}	6.02×10^{-14}
2	II	5.71×10^{-07}	1.67×10^{-06}	1.35×10^{-08}	9.58×10^{-13}
	III	6.19×10^{-06}	2.04×10^{-06}	1.47×10^{-06}	5.74×10^{-13}
	I	1.49×10^{-06}	3.74×10^{-06}	1.32×10^{-08}	2.67×10^{-13}
3	II	7.31×10^{-07}	2.41×10^{-06}	9.84×10^{-09}	7.92×10^{-13}
	III	5.80×10^{-07}	1.90×10^{-06}	1.94×10^{-09}	2.61×10^{-12}
	I	1.22×10^{-07}	2.78×10^{-07}	4.05×10^{-09}	2.62×10^{-14}
4	II	8.49×10^{-07}	2.71×10^{-06}	8.71×10^{-08}	1.02×10^{-12}
	III	3.19×10^{-07}	9.68×10^{-07}	9.41×10^{-09}	8.25×10^{-13}

D. EXAMPLE 4: RADIATIVE HEAT TRANSFER

In this example, the heat transfer is consider through radiation, ϵ_2, only. There is no heat transfer by convection ($\nu = 0$) and conduction ($\epsilon_1 = 0$). The example has three cases, in Case I radiation consider as $\epsilon_2 = 0.3$, for case II $\epsilon_2 = 0.6$ and for case III $\epsilon_2 = 0.9$. The input point is taken in [0, 1], so for N input points the fitness function given in equations (12)-(14) can updated as:

$$E_{c1} = \frac{1}{N}\sum_{m=1}^{N}\left(\frac{\mathrm{d}}{\mathrm{d}\eta}\left[\left(1+o.3\hat{\theta}_m\right)\frac{\mathrm{d}\hat{\theta}_m}{\mathrm{d}\eta}\right] - \nu^2\hat{\theta}_m - \varepsilon_2\hat{\theta}_m^4\right)^2$$

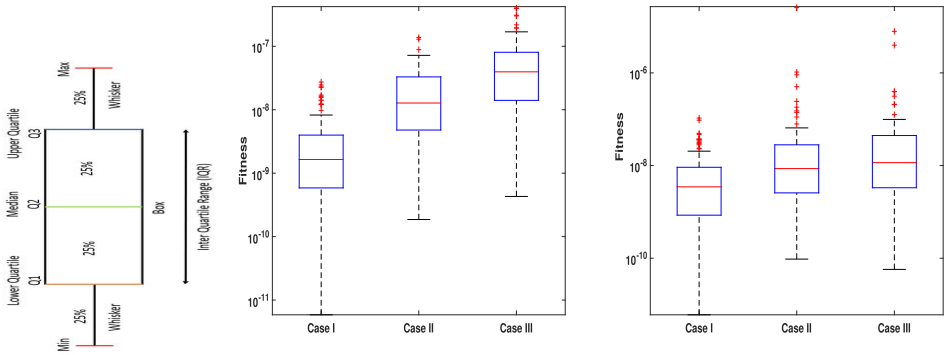

(a) Explanation of Box-plot (b) Fitness evaluation of Example 1 by Boxplot (c) Fitness evaluation of Example 2 by Boxplot

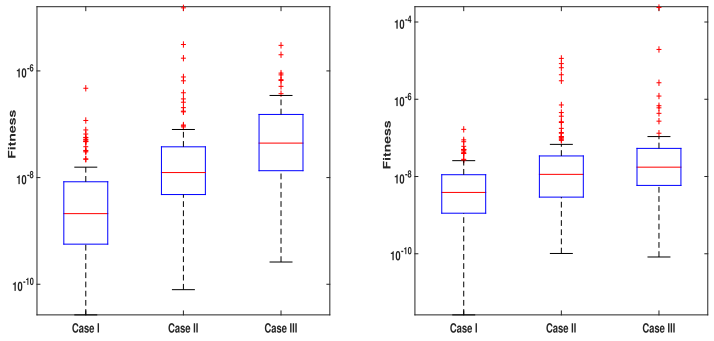

(d) Fitness evaluation of Example 3 by Boxplot (e) Fitness evaluation of Example 4 by Boxplot

FIGURE 13. **(b–e) shows fitness evaluation of all the examples with the help of Boxplots.**

$$+\frac{1}{2}\left(\left(\frac{\mathrm{d}\hat{\theta}}{\mathrm{d}\eta}(0)\right)^2+\left(\hat{\theta}(1)-1\right)^2\right), \tag{43}$$

$$E_{c2}=\frac{1}{N}\sum_{m=1}^{N}\left(\frac{\mathrm{d}}{\mathrm{d}\eta}\left[\left(1+0.6\hat{\theta}_m\right)\frac{\mathrm{d}\hat{\theta}_m}{\mathrm{d}\eta}\right]-\nu^2\hat{\theta}_m-\varepsilon_2\hat{\theta}_m^4\right)^2 +,\frac{1}{2}\left(\left(\frac{\mathrm{d}\hat{\theta}}{\mathrm{d}\eta}(0)\right)^2+\left(\hat{\theta}(1)-1\right)^2\right), \tag{44}$$

$$E_{c3}=\frac{1}{N}\sum_{m=1}^{N}\left(\frac{\mathrm{d}}{\mathrm{d}\eta}\left[\left(1+0.9\hat{\theta}_m\right)\frac{\mathrm{d}\hat{\theta}_m}{\mathrm{d}\eta}\right]-\nu^2\hat{\theta}_m-\varepsilon_2\hat{\theta}_m^4\right)^2 +\frac{1}{2}\left(\left(\frac{\mathrm{d}\hat{\theta}}{\mathrm{d}\eta}(0)\right)^2+\left(\hat{\theta}(1)-1\right)^2\right), \tag{45}$$

as the minimization is done by ANN-SCA-IPA algorithm for the solution of this example with minimum errors. The best unknown variable called weights of ANN found is plugged in equation (9) to get the solution. For the set of appropriate weights, 30 neurons are considered. The solution for each case is given as:

$$\hat{\theta}_{cI}=\frac{0.740626025894499}{1+\mathrm{e}^{-(1.881160691354930\eta+10.000963464832500)}}+\cdots +\frac{2.672372291277010}{1+\mathrm{e}^{-(-0.126257598731503\eta-8.083346766188970)}}, \tag{46}$$

$$\hat{\theta}_{cII}=\frac{-0.413050771467862}{1+\mathrm{e}^{-(-0.097399610214508\eta+1.576311218280620)}}+\cdots +\frac{7.768326648634920}{1+\mathrm{e}^{-(3.932241622308430\eta-10.558713541440500)}}, \tag{47}$$

$$\hat{\theta}_{cIII}=\frac{0.515927409162672}{1+\mathrm{e}^{-(0.591516053509152\eta-0.343623553964357)}}+\cdots +\frac{4.627043351605150}{1+\mathrm{e}^{-(4.892305232807030\eta-10.799738153365600)}}, \tag{48}$$

the full form of Equations (46)–(48) is given in the Appendix for up to 14-decimal places. The approximated solutions are graphically compared with the solution of Runge–Kutta order 4 (RK4) shown in Figure 7a. The solution is plotted with step size 0.1 in interval [0, 1]. The weights are also drawn with 3D bar graphs in figure 7(b–c). The weights are also reported in table 4. The dots (·) show the results of RK4, and the solid lines represent approximated solutions. The overlapping of these solutions shows the convergence of ANN-SCA-IPA algorithm.

VIII. EVALUATION OF ANN-SCA-IPA ALGORITHM

To verify the consistency, reliability, and convergence of the proposed ANN–SCA–IPA algorithm. The statistical operators are utilized as defined and discussed in section VI. The values of the statistic operators MAD, RMSE, and ENSE is drawn with a line graph having semi–log on y-axis. Additionally, in a similar manner, the fitness of each case is also drawn. The algorithm is executed 100 times to collect large data set because few runs cannot verify the capability of a technique. The data is arranged in descending order to observe the small variation as well in the data. Figure 8 shows data for MAD of each example. From figure 8a it can observe that the values of MAD in example 1 are varies between $10^{-5} - 10^{-8}$, figure 8b shows MAD data for example 2 which lies between $10^{-1} - 10^{-4}$, figure 8c shows data of example 3 which lies in between $10^{-2} - 10^{-5}$ and similarly from figure 8d data of example 4 can be observed.

In figure 9, the RMSE data of all the four examples are drawn. It can observe that the values in the data lie in $10^{-2} - 10^{-8}$ for all examples. Similarly, in figure 10 data of ENSE is drawn. The figures show that out of 100 runs only on few runs, the performance of ANN-SCA-IPA algorithm is worst, which shows the reliability and consistency of the proposed technique.

Moreover, in figure 11, if the fitness data is observed it can seem that all runs have much better and considerable fitness, which concludes that according to fitness function, equation (12), the solutions have minimum errors. The fitness values lie between $10^{-4} - 10^{-12}$ for all examples.

For further evaluation, the minimum values of statistical operators MAD, RMSE, ENSE and Fitness are drawn by bar graph. It can clearly show the minimum values of the mentioned operators. In figure 12a,b example 1 and example 2 are drawn with horizontal bars while in figure 12c,d example 3 and 4 are drawn with vertical graphs, respectively. Each operator is drawn with a separate bar. For quartile evaluation of fitness, the fitness data is drawn with Boxplots. The explanation of Boxplot is given in sub-figure 13a, sub-figure 13b, sub-figure 13c and sub-figure 13d shows fitness interquartile range of fitness for example 1, 2, 3 and 4, respectively.

Additionally, the ANN-SCA-IPA algorithm is also assessed by global versions of performance operators as defined in section VI. The assessment data of global operators GMAD, GRMSE, GENSE, and GFIT is reported in table 5. The values of global operators depend on the average value of their respective operators. The table shows that the global performance operates validate the solutions of the proposed technique.

IX. CONCLUSION

In this work, the heat transfer problem is considered. Heat transfer dynamics is executed by variations of different ways of heat transfer such as conduction, convection, and radiation and loss of heat with the same rate of conduction, convection, and radiation. The transfer of heat is assumed in longitudinal Fin. The temperature at the bottom is assumed constant while on the tip of the fin, the heat transfer is negligible. Moreover on the surface of fin heat flows through convection and radiation. For quantitative analysis of heat transfer, a novel hybrid technique is proposed. The technique is a hybridization of population-based approach Sine-Cosine algorithm and local search technique Interior Point algorithm with the utilization of artificial neural network, namely ANN-SCA-IPA algorithm. The SCA generates multiple solutions according to its population size and assigns it to IPA as the initial point.

Furthermore, to validate reliability, consistency, and robustness of the ANN–SCA–IPA algorithm, a large data set is collected and is evaluated by performance operators. The data is drawn with a line graph having semi-log at y-axis. For convergence, the solutions of ANN–SCA–IPA algorithm is compared graphically with the numerical solutions of RK4. And the collected data is plotted by convergence graphs such as boxplot and bar-graphs. The proposed technique can solve more complex physical, chemical and biological problems.

X. ABBREVIATIONS

The following abbreviations are used in this manuscript:

HTM	Heat transfer model
MAD	Mean square error
RMSE	Root mean square error
ENSE	Error in Nash–Sutcliffe efficiency
ANN	Artificial neural network
SCA	Sine-Cosine Algorithm
IPA	Interior point algorithm
RK4	Runge-Kutta order four

APPENDIX A

Solution for Example 1 of HTM is as follows:(In subscripts c_I, c_II, and c_III represent case I, II, and III, respectively)

$$\hat{\theta}_{c_I}(\eta) = \frac{2.602626425199950}{1+\mathrm{e}^{-(0.017012265990431\eta-0.754708570112332)}} + \frac{1.410326813508950}{1+\mathrm{e}^{-(-0.106063731378422\eta-4.508911917589510)}} + \frac{9.991301864537020}{1+\mathrm{e}^{-(-0.488942546889799\eta+1.193186518993810)}} + \frac{-6.401536261568260}{1+\mathrm{e}^{-(0.373978998229374\eta+2.263369191898170)}} + \frac{-0.199172829074871}{1+\mathrm{e}^{-(-0.535537746258558\eta+0.139462002950955)}} + \frac{1.398017949953400}{1+\mathrm{e}^{-(-1.741125501404640\eta+7.045511245877330)}} + \frac{1.708310396440250}{1+\mathrm{e}^{-(0.156820720913337\eta-10.000149875877400)}} + \frac{1.235687488216280}{1+\mathrm{e}^{-(0.785900783916801\eta-1.083496764304090)}} + \frac{1.310664872117550}{1+\mathrm{e}^{-(-0.352371709696856\eta-0.920640239999641)}} + \frac{-3.691880668283030}{1+\mathrm{e}^{-(-0.741567080633551\eta+10.004971643282500)}}$$

$$\hat{\theta}_{c_{II}}(\eta) = \frac{-0.3579413314694420}{1+e^{-(0.2639144080139470\eta+9.9997537245370100)}} + \frac{-2.7240659334800700}{1+e^{-(-1.3037652032037300\eta-9.7046214046877400)}} + \frac{2.8583357161423800}{1+e^{-(-2.1244415564050700\eta+5.2964120173751900)}} + \frac{-0.1993785187736860}{1+e^{-(0.0043777354204988\eta-1.7967742455013300)}} + \frac{0.7146302195143110}{1+e^{-(1.8544579914479400\eta-2.9072841683593700)}} + \frac{-6.6432457934861000}{1+e^{-(6.7573317302018400\eta-14.3186978117044000)}} + \frac{0.6590720447013260}{1+e^{-(-2.2438845774674100\eta+7.9314329026897000)}} + \frac{-4.2749481585722800}{1+e^{-(0.1020417018459410\eta-9.9994988713727500)}} + \frac{-2.0823888848632600}{1+e^{-(0.7986615354064490\eta+1.0162777683356300)}} + \frac{-11.5140526176243000}{1+e^{-(0.8848756181363330\eta-2.8589463199225000)}}$$

$$\hat{\theta}_{c_{III}}(\eta) = \frac{-3.1600304212568400}{1+e^{-(0.7317636709211440\eta+0.0457636313129858)}} + \frac{-2.8294682173501800}{1+e^{-(-2.3302179258066300\eta-10.5056405123313000)}} + \frac{1.1288689813357000}{1+e^{-(-0.4304904622573220\eta+10.0011789496488000)}} + \frac{-5.6967436258632900}{1+e^{-(3.8593467737275000\eta-7.8828201882946100)}} + \frac{1.4577562571114400}{1+e^{-(-1.7431117896316800\eta+2.5376771583630400)}} + \frac{0.2530985993803010}{1+e^{-(1.8229107164804600\eta+10.1588267925447000)}} + \frac{1.4418951483637800}{1+e^{-(-6.1976860796540400\eta-9.6184580240629800)}} + \frac{-0.1373597559947500}{1+e^{-(-6.5847744302265500\eta-13.4288087499202000)}} + \frac{-1.7441311295403400}{1+e^{-(0.0386853158224262\eta-2.6548109627102400)}} + \frac{-5.3586709464080500}{1+e^{-(11.3094882974833000\eta-19.2041889362696000)}}$$

Example 2 all cases

$$\hat{\theta}_{c_I}(\eta) = \frac{-0.7220917771440140}{1+e^{-(1.0853456184342900\eta+7.1677135318354300)}} + \frac{0.0428079586607537}{1+e^{-(1.2606251848621300\eta+7.8684063184998200)}} + \frac{1.2396157107296600}{1+e^{-(0.3478667807996960\eta+10.0277113008724000)}} + \frac{-0.0017979640233192}{1+e^{-(3.8481847720312000\eta+0.9612988718656800)}} + \frac{2.1593741656159800}{1+e^{-(0.8679470621837150\eta-2.2537623419261700)}} + \frac{-2.1966860566177300}{1+e^{-(0.7790779418163660\eta-5.8623613935545400)}} + \frac{0.5121820763039080}{1+e^{-(-3.4557457481639300\eta-6.7471823689493900)}} + \frac{9.5394970783588000}{1+e^{-(2.6063399122940900\eta-8.2957141137283600)}} + \frac{6.3198410817587800}{1+e^{-(0.9783752717760270\eta-10.4341936974731000)}} + \frac{-4.9523984509801100}{1+e^{-(3.0725965025060200\eta-9.2893864166213300)}}$$

$$\hat{\theta}_{c_{II}}(\eta) = \frac{0.7756231927533090}{1+e^{-(0.8031281436684710\eta-0.1148112091070760)}} + \frac{-0.6206709375419610}{1+e^{-(0.1190259422918990\eta-0.2013593416227720)}} + \frac{-1.4118583811919000}{1+e^{-(-0.8494127357314550\eta+2.4980489328084000)}} + \frac{3.9680743492330000}{1+e^{-(3.2481624188195000\eta-9.2236145308858400)}} + \frac{-1.6164897025228400}{1+e^{-(0.0561425141102149\eta-0.5750453345101440)}} + \frac{-0.1924529783872820}{1+e^{-(-0.4813062917533250\eta+7.4778577559415400)}} + \frac{-2.1162988765120100}{1+e^{-(-0.2694777164412590\eta+0.1631069103709620)}} + \frac{5.0500252713098200}{1+e^{-(2.6063399122940900\eta-8.2957141137283600)}} + \frac{6.3198410817587800}{1+e^{-(0.9783752717760270\eta-10.4341936974731000)}} + \frac{-4.9523984509801100}{1+e^{-(3.0725965025060200\eta-9.2893864166213300)}}$$

$$\hat{\theta}_{c_{III}}(\eta) = \frac{-3.111663113555700}{1+e^{-(-0.558620574697884\eta-3.000802607145150)}} + \frac{0.303057980143337}{1+e^{-(-1.356472894010720\eta+1.336212933214470)}} + \frac{-1.137469061715660}{1+e^{-(1.040923185541890\eta-8.316549305769940)}} + \frac{7.111697118010730}{1+e^{-(4.121806835523890\eta-10.782349700965400)}} + \frac{-8.545447100250290}{1+e^{-(-0.197123055241083\eta-10.234710224360200)}} + \frac{1.469070302679980}{1+e^{-(2.140619299304930\eta-4.579447334610990)}} + \frac{-1.193946580086190}{1+e^{-(-0.004157775408407\eta-3.182229399530200)}} + \frac{-4.641431878588000}{1+e^{-(-0.035017099297094\eta-6.329849638763660)}} + \frac{2.062616055371330}{1+e^{-(1.058041159402040\eta-1.381869547871840)}} + \frac{-0.061571364069443}{1+e^{-(-0.288392390204304\eta-5.097840894490520)}}$$

Example 3 all cases

$$\hat{\theta}_{c_I} = \frac{-0.953645918137492}{1+e^{-(-0.248134998131578\eta+0.134914168705997)}} + \frac{-8.129060014944370}{1+e^{-(0.053657407976731\eta-4.715172763269860)}}$$

$$+\frac{-0.178446851181089}{1+e^{-(3.682855432683080\eta+7.513742006348150)}}+\frac{6.739569607024550}{1+e^{-(1.270995581582090\eta-4.170503380488740)}}+\frac{-0.006244031217162}{1+e^{-(0.054968064279487\eta+10.000000010412700)}}+\frac{0.875654213097466}{1+e^{-(-0.676129206808785\eta-0.387805562563759)}}+\frac{3.734510096548330}{1+e^{-(0.845766411548374\eta-2.967241582558870)}}+\frac{0.003204956616999}{1+e^{-(-0.634477217539597\eta+9.999931104997040)}}+\frac{1.812954569411820}{1+e^{-(0.461490536611498\eta-0.882652198134721)}}+\frac{5.721740039401010}{1+e^{-(2.349323748129270\eta-8.427192539483040)}}$$

$$\hat{\theta}_{cII}=\frac{-0.078268222639117}{1+e^{-(2.610437044720450\eta+10.004957232882700)}}+\frac{0.523288269674844}{1+e^{-(-1.615401365157810\eta+4.030350474313750)}}+\frac{19.691374656079000}{1+e^{-(2.307568242111670\eta-6.635522252039310)}}+\frac{6.072945319614970}{1+e^{-(0.310233954043648\eta+-10.048500643552800)}}+\frac{5.870871618800980}{1+e^{-(1.429421557095450\eta-3.281179911621350)}}+\frac{-2.701499778209620}{1+e^{-(0.001065614477865\eta+1.036031829189730)}}+\frac{1.548295501590430}{1+e^{-(-0.424539599556127\eta+5.549635270318570)}}+\frac{-6.412924448018040}{1+e^{-(-1.047395732800670\eta-12.549803212551200)}}+\frac{-1.444200746406220}{1+e^{-(-4.086520352460890\eta+-12.616677690485800)}}+\frac{-0.151288804822108}{1+e^{-(-0.251753983022694\eta-9.291174521828190)}}$$

$$\hat{\theta}_{cIII}=\frac{-1.011859279395540}{1+e^{-(-0.556578989183962\eta-8.243678366300250)}}+\frac{0.423323467680743}{1+e^{-(1.048188889545280\eta+6.241999464506500)}}+\frac{-1.258047052306320}{1+e^{-(-0.019961373402526\eta+0.618080945356904)}}+\frac{1.400285362835750}{1+e^{-(-2.295557297564900\eta-6.808511820087270)}}+\frac{-0.415314351708677}{1+e^{-(0.273505339622869\eta+1.980564227868040)}}+\frac{82.631319293463600}{1+e^{-(2.295653767156770\eta-7.061083612728530)}}+\frac{1.538364434376450}{1+e^{-(1.666621375988020\eta-3.046423817498670)}}+\frac{3.150686854700910}{1+e^{-(0.602110993817371\eta-7.483644680916230)}}+\frac{7.596076584513290}{1+e^{-(19.532510902947200\eta-45.962460205690600)}}+\frac{0.754189716078391}{1+e^{-(0.462451913859229\eta+8.017052181073470)}}$$

Example 4 all cases

$$\hat{\theta}_{cI}=\frac{0.740626025894499}{1+e^{-(1.881160691354930\eta+10.000963464832500)}}+\frac{1.036630953366560}{1+e^{-(0.002321294090145\eta-6.925756555777160)}}+\frac{0.638701290277219}{1+e^{-(-1.101545460200210\eta-3.822801351081940)}}+\frac{0.078728048824448}{1+e^{-(0.647114899295562\eta+7.586828795265160)}}+\frac{8.449640211933960}{1+e^{-(1.478212047040960\eta-5.898974679461190)}}+\frac{0.045644823646597}{1+e^{-(-0.024893046779482\eta+2.076944762812710)}}+\frac{0.979432739565070}{1+e^{-(3.609790705887980\eta-9.836883018211550)}}+\frac{1.487561926994920}{1+e^{-(0.656354827622091\eta-1.551061672119390)}}+\frac{-0.674664834728253}{1+e^{-(0.287872355290101\eta+0.088422704660012)}}+\frac{2.672372291277010}{1+e^{-(-0.126257598731503\eta-8.083346766188970)}}$$

$$\hat{\theta}_{cII}=\frac{-0.413050771467862}{1+e^{-(-0.097399610214508\eta+1.576311218280620)}}+\frac{-9.061687751983110}{1+e^{-(-0.104392935792038\eta-2.332855950695870)}}+\frac{-0.194159763128724}{1+e^{-(0.077040544327816\eta-0.308316106777158)}}+\frac{1.219777816267520}{1+e^{-(-0.668409668137094\eta-1.772307678754570)}}+\frac{7.954751375615440}{1+e^{-(1.456382886653830\eta-5.070008882958910)}}+\frac{0.445308977083408}{1+e^{-(-0.148963381818654\eta-1.121047930200200)}}+\frac{0.530273287315192}{1+e^{-(1.332651780577180\eta+9.009647020125680)}}+\frac{-0.077146313606151}{1+e^{-(0.184348009844110\eta-0.997507201455261)}}+\frac{2.950438271607060}{1+e^{-(0.193513027147217\eta-0.529558886935442)}}+\frac{7.768326648634920}{1+e^{-(3.932241622308430\eta-10.558713541440500)}}$$

$$\hat{\theta}_{cIII}=\frac{0.515927409162672}{1+e^{-(0.591516053509152\eta-0.343623553964357)}}+\frac{10.048753219767600}{1+e^{-(0.633592169104042\eta-3.739199129558130)}}+\frac{0.249734326593041}{1+e^{-(0.038889874917238\eta-3.438844807486750)}}+\frac{1.260313002261930}{1+e^{-(2.299734850222970\eta-4.646496135432730)}}+\frac{0.218249905802003}{1+e^{-(-0.923139237284723\eta-0.412801360557520)}}$$

$$+\frac{0.107569611727710}{1+e^{-(-0.095840428321070\eta+5.900530196062090)}}$$
$$+\frac{-0.221338262972027}{1+e^{-(-0.434280971227803\eta-6.600471154450340)}}$$
$$+\frac{-0.463336882159176}{1+e^{-(-0.134620663655608\eta-4.602273477252520)}}$$
$$+\frac{0.006749072245445}{1+e^{-(0.001354288705585\eta-3.298067582919490)}}$$
$$+\frac{4.627043351605150}{1+e^{-(4.892305232807030\eta-10.799738153365600)}}$$

REFERENCES

[1] B. Abu-Jdayil, A.-H. Mourad, W. Hittini, M. Hassan, and S. Hameedi, "Traditional, state-of-the-art and renewable thermal building insulation materials: An overview," *Construct. Building Mater.*, vol. 214, pp. 709–735, Jul. 2019.

[2] S.-R. Yan, M. Izadi, M. A. Sheremet, I. Pop, H. F. Oztop, and M. Afrand, "Inclined Lorentz force impact on convective-radiative heat exchange of micropolar nanofluid inside a porous enclosure with tilted elliptical heater," *Int. Commun. Heat Mass Transf.*, vol. 117, Oct. 2020, Art. no. 104762.

[3] M. Izadi, H. F. Oztop, M. A. Sheremet, S. A. M. Mehryan, and N. Abu-Hamdeh, "Coupled FHD–MHD free convection of a hybrid nanoliquid in an inversed T-shaped enclosure occupied by partitioned porous media," *Numer. Heat Transf., A, Appl.*, vol. 76, no. 6, pp. 479–498, Sep. 2019.

[4] M. Izadi, M. Javanahram, S. M. H. Zadeh, and D. Jing, "Hydrodynamic and heat transfer properties of magnetic fluid in porous medium considering nanoparticle shapes and magnetic field-dependent viscosity," *Chin. J. Chem. Eng.*, vol. 28, no. 2, pp. 329–339, Feb. 2020.

[5] M. Izadi, M. A. Sheremet, and S. A. M. Mehryan, "Natural convection of a hybrid nanofluid affected by an inclined periodic magnetic field within a porous medium," *Chin. J. Phys.*, vol. 65, pp. 447–458, Jun. 2020.

[6] C. Qi, J. Tang, F. Fan, and Y. Yan, "Effects of magnetic field on thermo-hydraulic behaviors of magnetic nanofluids in CPU cooling system," *Appl. Thermal Eng.*, vol. 179, Oct. 2020, Art. no. 115717.

[7] S. Mishra, B. Mahanthesh, J. Mackolil, and P. K. Pattnaik, "Nonlinear radiation and cross-diffusion effects on the micropolar nanoliquid flow past a stretching sheet with an exponential heat source," *Heat Transf.*, vol. 50, no. 4, pp. 3530–3546, Jun. 2021.

[8] B. Mahanthesh and K. Thriveni, "Significance of inclined magnetic field on nano-bioconvection with nonlinear thermal radiation and exponential space based heat source: A sensitivity analysis," *Eur. Phys. J. Special Topics*, pp. 1487–1501, Apr. 2021.

[9] P. Rana, W. Al-Kouz, B. Mahanthesh, and J. Mackolil, "Heat transfer of TiO_2–EG nanoliquid with active and passive control of nanoparticles subject to nonlinear Boussinesq approximation," *Int. Commun. Heat Mass Transf.*, vol. 126, Jul. 2021, Art. no. 105443.

[10] M. Nazeer, F. Hussain, M. I. Khan, Asad-Ur-Rehman, E. R. El-Zahar, Y.-M. Chu, and M. Y. Malik, "Theoretical study of MHD electro-osmotically flow of third-grade fluid in micro channel," *Appl. Math. Comput.*, vol. 420, May 2022, Art. no. 126868.

[11] J. Wang, M. Ijaz Khan, W. A. Khan, S. Z. Abbas, and M. I. Khan, "Transportation of heat generation/absorption and radiative heat flux in homogeneous–heterogeneous catalytic reactions of non-newtonian fluid (Oldroyd-B model)," *Comput. Methods Programs Biomed.*, vol. 189, Jun. 2020, Art. no. 105310.

[12] T. Hayat, M. Tamoor, M. I. Khan, and A. Alsaedi, "Numerical simulation for nonlinear radiative flow by convective cylinder," *Results Phys.*, vol. 6, pp. 1031–1035, Jan. 2016.

[13] S. Qayyum, M. I. Khan, T. Hayat, and A. Alsaedi, "Comparative investigation of five nanoparticles in flow of viscous fluid with Joule heating and slip due to rotating disk," *Phys. B, Condens. Matter*, vol. 534, pp. 173–183, Apr. 2018.

[14] M. I. Khan, T. Hayat, M. Waqas, and A. Alsaedi, "Outcome for chemically reactive aspect in flow of tangent hyperbolic material," *J. Mol. Liquids*, vol. 230, pp. 143–151, Mar. 2017.

[15] S. Unger, M. Beyer, S. Gruber, R. Willner, and U. Hampel, "Experimental study on the air-side thermal-flow performance of additively manufactured heat exchangers with novel fin designs," *Int. J. Thermal Sci.*, vol. 146, Dec. 2019, Art. no. 106074.

[16] A. J. Modi and M. K. Rathod, "Comparative study of heat transfer enhancement and pressure drop for fin-and-circular tube compact heat exchangers with sinusoidal wavy and elliptical curved rectangular winglet vortex generator," *Int. J. Heat Mass Transf.*, vol. 141, pp. 310–326, Oct. 2019.

[17] T. Ambreen, A. Saleem, H. M. Ali, S. A. Shehzad, and C. W. Park, "Performance analysis of hybrid nanofluid in a heat sink equipped with sharp and streamlined micro pin-fins," *Powder Technol.*, vol. 355, pp. 552–563, Oct. 2019.

[18] T. U. Shinde, V. H. Dalvi, C. S. Mathpati, N. Shenoy, S. V. Panse, and J. B. Joshi, "Heat transfer investigation of PCM pipe bank thermal storage for space heating application," *Chem. Eng. Process. Process Intensification*, Jan. 2022, Art. no. 108791.

[19] I. Zaaroura, S. Harmand, J. Carlier, M. Toubal, A. Fasquelle, and B. Nongaillard, "Thermal performance of self-rewetting gold nanofluids: Application to two-phase heat transfer devices," *Int. J. Heat Mass Transf.*, vol. 174, Aug. 2021, Art. no. 121322.

[20] J. Huang, C. Wang, K. Guo, D. Zhang, G. H. Su, W. Tian, and S. Qiu, "Heat transfer analysis of heat pipe cooled device with thermoelectric generator for nuclear power application," *Nucl. Eng. Design*, vol. 390, Apr. 2022, Art. no. 111652.

[21] H. Ullah, T. Hayat, S. Ahmad, and M. S. Alhodaly, "Entropy generation and heat transfer analysis in power-law fluid flow: Finite difference method," *Int. Commun. Heat Mass Transf.*, vol. 122, Mar. 2021, Art. no. 105111.

[22] M. Sandberg, O. Yuksel, I. Baran, J. H. Hattel, and J. Spangenberg, "Numerical and experimental analysis of resin-flow, heat-transfer, and cure in a resin-injection pultrusion process," *Compos. A, Appl. Sci. Manuf.*, vol. 143, Apr. 2021, Art. no. 106231.

[23] S. Ahmad, T. Hayat, A. Alsaedi, H. Ullah, and F. Shah, "Computational modeling and analysis for the effect of magnetic field on rotating stretched disk flow with heat transfer," *Propuls. Power Res.*, vol. 10, no. 1, pp. 48–57, Mar. 2021.

[24] T. Liu, Y. Li, Q. Jing, Y. Xie, and D. Zhang, "Supervised learning method for the physical field reconstruction in a nanofluid heat transfer problem," *Int. J. Heat Mass Transf.*, vol. 165, Feb. 2021, Art. no. 120684.

[25] N. Zobeiry and K. D. Humfeld, "A physics-informed machine learning approach for solving heat transfer equation in advanced manufacturing and engineering applications," *Eng. Appl. Artif. Intell.*, vol. 101, May 2021, Art. no. 104232.

[26] S. Güngör, U. Ceyhan, and Z. H. Karadeniz, "Optimization of heat transfer in a grooved pipe model by stochastic algorithms and DOE based RSM," *Int. J. Thermal Sci.*, vol. 159, Jan. 2021, Art. no. 106634.

[27] A. Ahmad, M. Sulaiman, A. Alhindi, and A. J. Aljohani, "Analysis of temperature profiles in longitudinal fin designs by a novel neuroevolutionary approach," *IEEE Access*, vol. 8, pp. 113285–113308, 2020.

[28] T. Zhao, M. I. Khan, and Y. Chu, "Artificial neural networking (ANN) analysis for heat and entropy generation in flow of non-Newtonian fluid between two rotating disks," *Math. Methods Appl. Sci.*, Apr. 2021.

[29] A. Ahmad, M. Sulaiman, and P. Kumam, "Solutions of fractional order differential equations modeling temperature distribution in convective straight fins design," *Adv. Difference Equ.*, vol. 2021, no. 1, pp. 1–38, Dec. 2021.

[30] N. A. Khan, O. I. Khalaf, C. A. T. Romero, M. Sulaiman, and M. A. Bakar, "Application of intelligent paradigm through neural networks for numerical solution of multiorder fractional differential equations," *Comput. Intell. Neurosci.*, vol. 2022, pp. 1–16, Jan. 2022.

[31] N. A. Khan, M. Sulaiman, C. A. T. Romero, G. Laouini, and F. S. Alshammari, "Study of rolling motion of ships in random beam seas with nonlinear restoring moment and damping effects using neuroevolutionary technique," *Materials*, vol. 15, no. 2, p. 674, Jan. 2022.

[32] A. F. Attia, R. A. El Sehiemy, and H. M. Hasanien, "Optimal power flow solution in power systems using a novel sine-cosine algorithm," *Int. J. Electr. Power Energy Syst.*, vol. 99, pp. 331–343, Jun. 2018.

[33] I. U. Rahman, M. Sulaiman, F. K. Alarfaj, P. Kumam, and G. Laouini, "Investigation of non-linear MHD Jeffery–Hamel blood flow model using a hybrid metaheuristic approach," *IEEE Access*, vol. 9, pp. 163214–163232, 2021.

[34] M. F. Khan, M. Sulaiman, C. A. T. Romero, and A. Alkhathlan, "Falkner–Skan flow with stream-wise pressure gradient and transfer of mass over a dynamic wall," *Entropy*, vol. 23, no. 11, p. 1448, Oct. 2021.

[35] M. F. Khan, M. Sulaiman, C. A. T. Romero, and A. Alkhathlan, "A hybrid Metaheuristic based on neurocomputing for analysis of unipolar electrohydrodynamic pump flow," *Entropy*, vol. 23, no. 11, p. 1513, Nov. 2021.
[36] A. Muzzio, "Approximate solution for convective fins with variable thermal conductivity," *J. Heat Transf.*, vol. 98, no. 4, pp. 680–682, Nov. 1976.
[37] A. Aziz and F. Khani, "Convection–radiation from a continuously moving fin of variable thermal conductivity," *J. Franklin Inst.*, vol. 348, no. 4, pp. 640–651, May 2011.
[38] F. Khani, M. A. Raji, and H. H. Nejad, "Analytical solutions and efficiency of the nonlinear fin problem with temperature-dependent thermal conductivity and heat transfer coefficient," *Commun. Nonlinear Sci. Numer. Simul.*, vol. 14, no. 8, pp. 3327–3338, Aug. 2009.
[39] S. Kim and C.-H. Huang, "A series solution of the non-linear fin problem with temperature-dependent thermal conductivity and heat transfer coefficient," *J. Phys. D, Appl. Phys.*, vol. 40, no. 9, p. 2979, 2007.
[40] S. Mirjalili, "SCA: A sine cosine algorithm for solving optimization problems," *Knowl.-Based Syst.*, vol. 96, pp. 120–133, Mar. 2016.
[41] S. M. Mirjalili, S. Z. Mirjalili, S. Saremi, and A. Mirjalili, "Sine cosine algorithm: Theory, literature review, and application in designing bend photonic crystal waveguides," in *Nature-Inspired Optimizers*. Springer, 2020, pp. 201–217.
[42] S. Gupta and K. Deep, "A novel hybrid sine cosine algorithm for global optimization and its application to train multilayer perceptrons," *Int. J. Speech Technol.*, vol. 50, no. 4, pp. 993–1026, Apr. 2020.
[43] K. S. Reddy, L. K. Panwar, B. Panigrahi, and R. Kumar, "A new binary variant of sine–cosine algorithm: Development and application to solve profit-based unit commitment problem," *Arabian J. for Sci. Eng.*, vol. 43, no. 8, pp. 4041–4056, Aug. 2018.
[44] R. Kuo, J.-Y. Lin, and T. P. Q. Nguyen, "An application of sine cosine algorithm-based fuzzy possibilistic c-ordered means algorithm to cluster analysis," *Soft Comput.*, vol. 25, pp. 1–16, Mar. 2020.
[45] R. H. Byrd, M E. Hribar, and J. Nocedal, "An interior point algorithm for large-scale nonlinear programming," *SIAM J. Optim.*, vol. 9, no. 4, pp. 877–900, 1999.

MUHAMMAD FAWAD KHAN received the B.Sc. and Master of Science degrees in mathematics from the University of Peshawar, in 2013 and 2017, respectively, and the M.Phil. degree in mathematics from Abdul Wali Khan University Mardan, Mardan, in 2019, where he is currently pursuing the Ph.D. degree in mathematics. His research interests include optimization algorithms, design engineering optimization problems, real-world problems, smart grids, communications technology, heuristics, metaheuristics, multi-objective optimization, design engineering optimization problems, structural engineering optimization problems, linear programming, linear and non-linear least squares optimization problems, artificial neural networks, and differential equations and energy management.

MUHAMMAD SULAIMAN received the B.Sc. degree from the University of Peshawar, in 2004, the M.Sc. and M.Phil. degrees in mathematics from Quaid-i-Azam University, Islamabad, Pakistan, in 2007 and 2009, respectively, and the Ph.D. degree in mathematics from the University of Essex, U.K., in 2015. From 2009 to 2016, he was a Lecturer and from February 2016 to August 2021, he was an Assistant Professor with Abdul Wali Khan University Mardan, Pakistan. Since August 2021, he has been promoted as an Associate Professor (Tenured) with the Department of Mathematics, Abdul Wali Khan University Mardan. He is the author of two book chapters and more than 59 research articles. His research interests include mathematical optimization techniques, global optimization, evolutionary algorithms, heuristics, metaheuristics, multi-objective optimization, design engineering optimization problems, structural engineering optimization problems, linear programming, linear and non-linear least squares optimization problems, evolutionary algorithms, nature-inspired metaheuristics, artificial neural networks, and differential equations. He is an Associate Editor of the journal *COJ Reviews and Research*, *SCIREA Journal of Mathematics*, *Annals of Applied Sciences*, and *Journal of Innovative Mathematics Learning*. For more information please visit: (www.msulaiman.org).

CARLOS ANDRÉS TAVERA ROMERO received the Doctor of Engineering degree from the Universidad del Valle, Cali, Colombia, South America. He was a Postdoctoral Fellow at the Universidad de San Buenaventura-Universidad Autónoma de Occidente. He is currently a Systems Engineer at the Universidad del Valle. He is a full-time Professor at the Santiago de Cali University, a Principal Researcher at the COMBA Research and Development Laboratory Research Group, and the Leader of the computer systems development research line. His main research interests include simulation of systems with discrete mechanisms, development of information systems, information technologies, and software engineering.

FAHAD SAMEER ALSHAMMARI received the master's and Ph.D. degrees from The University of Queensland. At various times in his career, he has taught, full-time, in intermediate and secondary schools, for a total of three years. He has taught in three universities, located in two nations (Saudi Arabia and Australia). He is the Head of the Department of Mathematics, College of Science, Prince Sattam Bin Abdulaziz University, Saudi Arabia, since August 2020. He is currently an Assistant Professor with the Department of Mathematics, Prince Sattam Bin Abdulaziz University. He has served as a Consultant and a Researcher in Saudi Arabia, Australia, India, Pakistan, and Bangladesh. He has published his fundamental research articles in several peer-reviewed international and national journals. He has participated and presented his research findings at many national and international conferences. His research interests include mathematical modeling, mathematical optimization techniques, field of algebra, quantum physics and mathematical physics, solitary wave solution of nonlinear PDEs, topological spaces, and its applications. He has been a member with the Australian Mathematical Society (AustMS), since April 2014.